(12)

CHEMICAL
RESEARCH,
DEVELOPMENT &
ENGINEERING
CENTER

CRDEC-CR-87021

AD-A176 297

FINITE ELEMENT CALCULATIONS OF VISCOELASTIC FLUID FLOW IN A SPINNING AND NUTATING CYLINDER

by S. Rosenblat
A. Gooding
M. S. Engleman

FLUID DYNAMICS INTERNATIONAL, INC.
Evanston, IL 60201

December 1986

U.S. ARMY
ARMAMENT
MUNITIONS
CHEMICAL COMMAND

Aberdeen Proving Ground, Maryland 21010-5423

Disclaimer

The findings in this report are not to be construed as an official Department of the Army position unless so designated by other authorizing documents.

Distribution Statement

Approved for public release; distribution is unlimited.

UNCLASSIFIED

SECURITY CLASSIFICATION OF THIS PAGE

REPORT DOCUMENTATION PAGE

1a. REPORT SECURITY CLASSIFICATION UNCLASSIFIED	1b. RESTRICTIVE MARKINGS
2a. SECURITY CLASSIFICATION AUTHORITY	3. DISTRIBUTION/AVAILABILITY OF REPORT Approved for public release; distribution is unlimited.
2b. DECLASSIFICATION/DOWNGRADING SCHEDULE	
4. PERFORMING ORGANIZATION REPORT NUMBER(S) CRDEC-CR-87021	5. MONITORING ORGANIZATION REPORT NUMBER(S)
6a. NAME OF PERFORMING ORGANIZATION Fluid Dynamics International, Inc. — 6b. OFFICE SYMBOL (If applicable)	7a. NAME OF MONITORING ORGANIZATION
6c. ADDRESS (City, State, and ZIP Code) 1600 Orrington Ave., Suite 505 Evanston, IL 60201	7b. ADDRESS (City, State, and ZIP Code)
8a. NAME OF FUNDING/SPONSORING ORGANIZATION CRDEC — 8b. OFFICE SYMBOL (If applicable) SMCCR-RSP-A	9. PROCUREMENT INSTRUMENT IDENTIFICATION NUMBER DAAK11-85-C-0012
8c. ADDRESS (City, State, and ZIP Code) Aberdeen Proving Ground, MD 21010-5423	10. SOURCE OF FUNDING NUMBERS PROGRAM ELEMENT NO. — PROJECT NO — TASK NO. — WORK UNIT ACCESSION NO

11. TITLE (Include Security Classification)

Finite Element Calculations of Viscoelastic Fluid Flow in a Spinning and Nutating Cylinder

12. PERSONAL AUTHOR(S)

Rosenblat, S., Cooding, A., and Engleman, M.S.

13a. TYPE OF REPORT	13b. TIME COVERED	14. DATE OF REPORT (Year, Month, Day)	15. PAGE COUNT
Contractor	FROM 85/01 TO 86/04	1986 December	97

16. SUPPLEMENTARY NOTATION

COR: Miles C. Miller, SMCCR-RSP-A, (301) 671-2186

17. COSATI CODES		
FIELD	GROUP	SUB-GROUP
01	01	
20	04	

18. SUBJECT TERMS (Continue on reverse if necessary and identify by block number)

Liquid-Filled Projectiles — Aeroballistics
Flight Stability — Viscoelastic Fluids

19. ABSTRACT (Continue on reverse if necessary and identify by block number)

An investigation has been performed of the flow of a non-Newtonian liquid in a spinning and nutating cylinder. An approximate analysis has been effected on the assumption that the radio of coning rate to spin rate is small and applied to the case of a cylinder of infinite length. A numerical calculation has been performed for the actual flow of two specified non-Newtonian liquids, using the finite element code FIDAP. Results are presented in both graphical and tabular form showing flow fields and calculated values of the despin moment for ranges of parameters. The question of appropriate representation of the liquid's non-Newtonian behavior is discussed.

20. DISTRIBUTION/AVAILABILITY OF ABSTRACT	21. ABSTRACT SECURITY CLASSIFICATION
☐ UNCLASSIFIED/UNLIMITED ☐ SAME AS RPT ☒ DTIC USERS	UNCLASSIFIED
22a. NAME OF RESPONSIBLE INDIVIDUAL TIMOTHY E. HAMPTON	22b. TELEPHONE (Include Area Code) (301) 671-2914 — 22c. OFFICE SYMBOL SMCCR-SPS-T

DD FORM 1473, 84 MAR — 83 APR edition may be used until exhausted. All other editions are obsolete.

SECURITY CLASSIFICATION OF THIS PAGE

UNCLASSIFIED

PREFACE

The work described in this report was authorized under Contract No. DAAK11-85-C-0012. This work was started in January 1985 and completed in April 1986.

The use of trade names or manufacturers' names in this report does not constitute an official endorsement of any commercial products. This report may not be cited for purposes of advertisement.

Acknowledgments

The authors express their considerable indebtedness to Miles Miller for many stimulating discussions and important insights and to Thorwald Herbert for several useful conversations.

Blank

CONTENTS

Blank

FINITE ELEMENT CALCULATIONS OF VISCOELASTIC FLUID FLOW IN A SPINNING AND NUTATING CYLINDER

1. INTRODUCTION

In recent years there has been considerable interest in understanding the onset of instability in liquid-filled shells that are simultaneously spinning and nutating in flight. Field observations by D'Amico and Miller (1979) indicate that there is an instability which appears in fluids of very high viscosity, and is therefore unrelated to the instability associated with the presence of inertial waves in fluids of very low viscosity (Stewartson 1959, Wedemeyer 1966). Theoretical work by Vaughn et al (1985) and Herbert (1985), coupled with the experiments of Miller (1982) performed under controlled conditions, confirm the presence of this high-viscosity instability, which manifests itself through a relatively large despin moment (leading to a loss in spin rate). It is generally thought that the despin moment attains a maximum at a fairly high viscosity value (low Reynolds number) and then decreases as the viscosity decreases.

Hitherto all work on this problem, both experimental and theoretical, has been restricted to Newtonian liquids. There are, however, practical reasons that make it important to consider the behavior and response of the spinning-nutating system when the liquid fill is non-Newtonian, and the present project is directed at comprehending and resolving the issues that arise in that case.

The primary purpose of this project was to determine the liquid-induced despin moment for the configuration shown in Figure 1. A right circular cylinder of length $2c$ and diameter $2a$ spins about its axis with angular speed ω. The axis of the cylinder is inclined to the vertical at the

nutation angle θ and rotates about the vertical with angular speed Ω. The cylinder is completely filled with a liquid of constant density ρ; this liquid is non-Newtonian, and the implications of this will be discussed in Section 2 below, but the liquid is taken to have a zero-shear-rate viscosity μ_0. The two axes of rotation intersect at the point O on the center line of the cylinder.

This report is organized in the following way. In Section 2 we discuss properties of non-Newtonian fluids that could be relevant to the present study, and describe a number of possible theoretical models that can be used. The general equations that govern the motion of the liquid, and the associated boundary conditions, are developed in Section 3, where appropriate nondimensionalizations are also introduced. Then in Section 4 we derive the expressions for the liquid-induced moments acting on the cylinder, and infer a general relationship between two of the components of the moment.

The work performed in this project has proceeded along two distinct but related paths. On the one hand we have developed an analytical treatment of the problem in the case of a cylinder of infinite length, following the procedure of Herbert (1985) for the Newtonian liquid case. The infinite length model has validity when the aspect ratio of the cylinder is large, which is frequently the case in flight and laboratory tests, and can predict the flow field except close to the cylinder ends. A reasonable estimate of the despin moment can also be obtained. The procedure and results are outlined in Sections 5 and 6 respectively. The method of analysis utilizes the fact that the nutation angle θ is generally quite

small ($|\theta| \leq 20°$), and that the ratio of angular velocities (Ω/ω) is also quite small. These facts enable the solution of the problem to be found by analytic perturbation techniques, as was done by Herbert (1985) for the Newtonian liquid case. In performing this analysis we were able to assess the contribution to the despin moment arising from the liquid's viscoelasticity, and to show how this contribution, from a theoretical point of view, depends on the constitutive model used to represent the non-Newtonian behavior.

In parallel with the perturbation analysis we have performed a numerical simulation of the flow in the cylinder shown in Figure 1, and have computed the moments. The computations were done using a task-oriented version of the finite-element code FIDAP; this code and the methodology of the simulations are described in Section 7. The properties of the non-Newtonian fluids to be simulated were deduced from data supplied by CRDC, as were the parameter ranges of interest. The results of the computations are presented in Section 8.

The results obtained are reviewed and discussed in Section 9.

2. NON-NEWTONIAN LIQUIDS

In attempting to model the flows of non-Newtonian liquids the fundamental difficulty always is the form of the relationship between the stress tensor and the deformation-rate (strain-rate) tensor, the so-called constitutive relation. No constitutive relation has been found, either empirically or from theory, that can claim to be appropriate for all flows of all non-Newtonian liquids. In fact, it is generally agreed that there is no such general constitutive relation or, if there is, it is so complex that it cannot be used for the solution of problems and cannot be determined empirically.

For modeling purposes, therefore, it follows that one is confronted with the more restricted task of determining a constitutive relation that applies to a limited class of flows and/or a limited class of fluids. If one asks whether it is possible to find a constitutive relation that describes all possible flows of one given non-Newtonian liquid, the answer, based on experience, is again negative. It turns out, on the other hand, that there are much better prospects of finding a constitutive relation to describe a limited class of flows for a reasonably wide range of fluids.

The consequence of this fact is that in studying a particular flow it is of primary importance to choose a constitutive relation that is appropriate to that flow. One aspect of this approach, however, needs to be carefully monitored. As will be seen below, constitutive relations always contain parameters that measure the viscoelastic properties of a liquid. These parameters have to be determined empirically, but the

determination has to be from experiments on the same class of flows for which the model is being constructed, since otherwise they may not be relevant to the particular constitutive relation being applied.

For example, it is well known that many polymer solutions exhibit shear thinning in plane, unidirectional shear flows; for such flows, and when no other fluid behavior is of interest, it is often sufficient to model shear thinning by introducing a shear-rate dependent viscosity function

$$\mu = \mu(\dot{\gamma}) \tag{2.1}$$

where $\dot{\gamma}$ is the magnitude of the rate of shear. From equation (2.1) one deduces a constitutive law

$$\underline{\tau} = \mu(\dot{\gamma})\underline{\dot{\gamma}} \tag{2.2}$$

which is an explicit relation between the stress tensor $\underline{\tau}$ and the rate of strain tensor $\underline{\dot{\gamma}}$. Various functional forms of equation (2.1) have been proposed, mostly involving algebraic dependence on $\dot{\gamma}$; a common form is the Carreau model

$$\frac{\mu - \mu_\infty}{\mu_0 - \mu_\infty} = \left[1 + (\lambda\dot{\gamma})^2\right]^{-\alpha} , \tag{2.3}$$

where μ_0 is zero-shear-rate viscosity, μ_∞ is infinite-shear-rate viscosity, λ is a time constant and α a power-law index.

While the constitutive relation implied by equation (2.2) can often be fitted quite well to experimental data on shear thinning in simple shearing flows, it is incapable of predicting other common viscoelastic effects, in particular normal stress difference and fluid elasticity.

For these and others it is usually necessary to go to a more sophisticated model. Thus, for example, the constitutive relation known as the second-order fluid model, typically written in the form

$$\underline{\tau} = \alpha_1 \dot{\underline{\gamma}} + \alpha_2 D\dot{\underline{\gamma}} - \alpha_{11} \dot{\underline{\gamma}} \cdot \dot{\underline{\gamma}} \quad , \tag{2.4}$$

where $\underline{\tau}$, $\dot{\underline{\gamma}}$ are the appropriate tensors, α_1, α_2 and α_{11} are constants, and D represents a convected or Jaumann derivative, predicts no shear thinning but does predict a normal stress difference and a complex viscosity in relaxation. Again, it should be emphasized, models such as (2.4) can be made to fit experimental observations only in a limited class of simple flow configurations. An improved version of equation (2.4) is the CEF model (Criminale et al, 1958) in which the constants α_1, α_2, α_{11} are replaced by (empirically determined) functions of shear rate.

A class of more widely acceptable models are the differential relations of the form

$$\underline{\tau} + \lambda D\underline{\tau} = 2\mu_0(\dot{\underline{\gamma}} + \epsilon\lambda D\dot{\underline{\gamma}}) \tag{2.5}$$

which contain a relaxation time constant λ, a zero-shear rate viscosity μ_0 and a retardation time constant $\epsilon\lambda$. The derivative D includes a parameter that changes the character of the model; the details will be discussed further below. This model (2.5) is known to be applicable over a wider class of flows than any of the others mentioned previously, but it is also known to be limited, and even unsatisfactory, when applied to very complicated flows.

In the present project we are dealing with a fully three-dimensional flow of a viscoelastic liquid. For three-dimensional flows there is virtually no information available, either experimental or theoretical, to determine whether one or any of the known constitutive relations is adequate to describe and predict the flow dynamics. This is because it is not known whether shear thinning, normal stress differences, elongational viscosity, stress relaxation, or some combination of all or some of these, plays the dominant role in any given three-dimensional flow. On this account a major thrust of this project has been the testing and categorizing of constitutive relations, with a view to eventual calibration against experiments, to ascertain what are the most important characteristics affecting the flow in a spinning and nutating cylinder. The object of this analysis was to arrive at a sufficiently accurate predictive constitutive relation that can be used for large-scale simulation. In Sections 5 and 6 of this work we describe the results of testing models such as those mentioned explicitly above, and draw some relevant conclusions.

The two principal (but by no means only) measures of the degree of "non-Newtonianness" of a liquid are the zero-shear-rate viscosity μ_0 and a time constant, denoted λ. The addition of certain polymers to a Newtonian liquid has the effect of increasing the viscosity, sometimes by orders of magnitude, so that μ_0 refers to the viscosity of the new, non-Newtonian liquid and is by no means the same as that of the solvent. For the case of liquid-filled shells at high (Newtonian) viscosity, this means that the new polymer solution must be regarded as having an even higher viscosity.

The time constant λ is a measure of the degree of shear thinning under deformation, as well as of normal stress and stress relaxation depending on the type of flow under consideration. To estimate how important any or all of these effects are in any given situation, one should compare the magnitude of λ (which has the dimensions of time) with some other typical time constant of the flow. In the present work an obvious candidate for the latter is the period of the spin, in which case we can define a dimensionless parameter We, called the Weissenberg number, by the formula

$$We = \lambda\omega \ . \tag{2.6}$$

Elastic effects become important when the elastic time constant is large compared with the dynamic time constant; this may well be the case in the present situation since the angular velocity of spin is quite large (4000-6000 r.p.m.).

For estimating the dynamical behavior of the liquid the appropriate dimensionless parameter is the Reynolds number

$$Re = \frac{\omega a^2 \rho}{\mu_0} \ . \tag{2.7}$$

Combining equations (2.6) and (2.7) we can define an alternative elastic parameter, called the Deborah number, by the formula

$$De = We/Re = \frac{\lambda \mu_0}{a^2 \rho} \tag{2.8}$$

which has the virtue that it is independent of spin rate, and represents the ratio of the elastic time constant to a typical diffusion time constant.

The parameters Re, We, De will play an important role in the subsequent discussion.

3. FORMULATION

As pointed out by Vaughn et al (1985) and Herbert (1985), it is convenient to write the governing equations in a nutating frame of reference, the so-called aeroballistic frame. In this coordinate system, the z-axis coincides with the axis of the cylinder, the x-axis lies in the plane containing the angular velocity vectors $\underline{\omega}$ and $\underline{\Omega}$, and the y-axis is perpendicular to this plane. This constitutes a right-handed cartesian system, with the origin taken at the center of the cylinder.

It is also convenient to use dimensionless forms of the governing equations. Nondimensionalization is achieved by scaling lengths with respect to the radius a, time with respect to the spin time constant ω^{-1}, linear velocities with respect to the speed $a\omega$, the angular velocity vector $\underline{\Omega}$ with respect to its magnitude Ω, the stress and deformation rate tensors with respect to $\mu_0\omega$ and ω respectively, and the pressure with respect to $\rho a^2\omega^2$. It is then easy to show that the governing equations for momentum and mass conservation with respect to the aeroballistic frame are

$$\underline{v}_t + \underline{v}\cdot\nabla\underline{v} + 2\eta\underline{\Omega}\times\underline{v} + \eta^2\underline{\Omega}\times(\underline{\Omega}\times\underline{r}) = -\nabla p + \frac{1}{\mathrm{Re}}\nabla\cdot\underline{\underline{\tau}} \tag{3.1}$$

$$\nabla\cdot\underline{v} = 0 \ . \tag{3.2}$$

The parameters appearing here are the Reynolds number, as defined by formula (2.7), and the spin ratio η

$$\eta = \Omega/\omega \ . \tag{3.3}$$

The dimensionless angular velocity vector $\underline{\Omega}$ with respect to the cartesian aeroballistic frame is

$$\underline{\Omega} = -\sigma\hat{\underline{i}} + \sqrt{1-\sigma^2}\,\hat{\underline{k}} \tag{3.4}$$

where

$$\sigma = \sin\theta \tag{3.5}$$

is the third crucial parameter of the problem. The boundary conditions are that the normal velocity component is zero at every rigid boundary and that the tangential velocity at a boundary is equal to the rigid-body velocity of that boundary. On physical grounds we require also that the velocity is bounded on the cylinder axis.

To complete the specification of the problem it is necessary to stipulate the constitutive relation between stress and strain rate. We shall consider a number of typical, representative relations all of which, it can be shown, are invariant with respect to the transformation from the inertial frame to the aeroballistic frame.

The dimensionless form of the constitutive relation corresponding to the power-law Carreau model (2.3) is

$$\underline{\underline{\tau}} = \frac{2\dot{\underline{\gamma}}}{[\epsilon + (1-\epsilon)(1 + We^2\,\dot{\gamma}^2)]^{\alpha}} \quad , \tag{3.6}$$

where We is defined by equation (2.6), $\epsilon = \mu_\infty/\mu_0$ and is often taken to be zero, and α is the power-law index. The strain-rate tensor in (3.6) is defined by

$$\dot{\underline{\gamma}} = \tfrac{1}{2}(\nabla\underline{v} + \nabla\underline{v}^{T}) \tag{3.7}$$

and $\dot{\gamma}$ is its magnitude.

The dimensionless form of the second-order fluid relation (2.4) is

$$\underline{\tau} = 2(\dot{\underline{\gamma}} - We\, D\dot{\underline{\gamma}} + 2\kappa\dot{\underline{\gamma}}\cdot\dot{\underline{\gamma}}) \quad , \tag{3.8}$$

where We is the Weissenberg number again and κ is a constant. The derivative D appearing in (3.8) is defined for a second-order tensor $\underline{p}$ by the formula,

$$D\underline{p} = \underline{p}_t + \underline{v}\cdot\nabla\underline{p} + \underline{\omega}\cdot\underline{p} - \underline{p}\cdot\underline{\omega} - a(\dot{\underline{\gamma}}\cdot\underline{p} + \underline{p}\cdot\dot{\underline{\gamma}}) \quad , \tag{3.9}$$

where $\underline{\omega}$ is the vorticity tensor

$$\underline{\omega} = \tfrac{1}{2}(\nabla\underline{v} - \nabla\underline{v}^T) \tag{3.10}$$

and a is a constant that can take values between -1 and $+1$. The choices $a = -1,0,+1$ reduce equation (3.9) to the lower convected, corotational and upper convected derivative respectively. It should be noted that (3.8) predicts no shear thinning in simple shear flow, but does predict constant first and second normal stress differences. The Weissenberg number that appears in (3.8), consequently, is a measure of the first normal stress difference and therefore may need to be interpreted differently from the corresponding parameter in (3.6), where it is a measure of shear thinning. The parameter κ in (3.8) is associated with the second normal stress difference.

A generalization of (3.8) is the Criminale-Ericksen-Filbey model, namely

$$\underline{\tau} = 2(\Phi_1(\dot{\gamma})\dot{\underline{\gamma}} - We\Phi_2(\dot{\gamma})D\dot{\underline{\gamma}} + 2\kappa\Phi_3(\dot{\gamma})\dot{\underline{\gamma}}\cdot\dot{\underline{\gamma}}) \quad , \tag{3.11}$$

where Φ_1, Φ_2, Φ_3 are generally empirically determined functions of $\dot{\gamma}$.

In particular, a suitably chosen form of Φ_1 can describe shear thinning effects, while the dependence of Φ_2 and Φ_3 on $\dot{\gamma}$ can describe the variation of first and second normal stress differences with shear rate.

A rather general differential model which we propose to study is

$$\underline{\tau} + \mathrm{We}\, D\underline{\tau} = 2(\dot{\underline{\gamma}} + \epsilon \mathrm{We}\, D\dot{\underline{\gamma}}) \tag{3.12}$$

where the operator D is defined by (3.9). This model predicts shear thinning when $-1 < a < 1$ and a shear-rate dependent first normal stress difference. It is a modified version of the Oldroyd (1958) 8-constant model. The Weissenberg number in this model is a measure of both shear thinning and normal stress, while $\epsilon = \mu_\infty / \mu_0$, as in (3.6).

It is convenient to introduce cylindrical polar coordinates (r,ϕ,z), defined by

$$x = r\cos\phi, \quad y = r\sin\phi, \quad z = z \ . \tag{3.13}$$

In that case the boundary conditions can be written simply as

$$\begin{aligned} &\underline{v} = \hat{\underline{\phi}} \quad \text{on } r = 1 \\ &\underline{v} = r\hat{\underline{\phi}} \quad \text{on } z = \pm b \\ &\underline{v} \text{ bounded as } r \to 0 \end{aligned} \tag{3.14}$$

where $b = c/a$ is the aspect ratio, while the angular velocity vector (3.4) takes the form

$$\underline{\Omega} = -\sigma\cos\phi\, \hat{\underline{r}} + \sigma\sin\phi\, \hat{\underline{\phi}} + \sqrt{1-\sigma^2}\, \hat{\underline{k}} \tag{3.15}$$

This completes the formulation of the problem.

4. MOMENTS

In this Section we discuss some issues concerning the moment acting on the cylinder shown in Figure 1, and derive an important relationship between two components of the moment vector. In the latter part of the Section we show what modifications are required when the problem of the infinitely long cylinder is being considered.

The total moment acting on the cylinder is denoted $\underline{M}_T^*$. Typical units are $gm \cdot cm^2 \cdot sec^{-2}$, and in conformity with the scalings introduced in Section 3 we define the dimensionless total moment $\underline{M}_T$ by the formula

$$\underline{M}_T^* = \rho a^5 \omega^2 \underline{M}_T \tag{4.1}$$

where ρ is fluid density, a is cylinder radius and ω is the spin rate. An expression for the moment can be written down in terms of pressure and stress fields, namely

$$\underline{M}_T = \int_V \underline{r} \times (-\nabla p + \frac{1}{Re} \nabla \cdot \underline{\underline{\tau}}) dV \tag{4.2}$$

or, equivalently,

$$\underline{M}_T = \int_S (-p\underline{r} \times d\underline{S} + \frac{1}{Re} \underline{r} \times \underline{\underline{\tau}} \cdot d\underline{S}) \tag{4.3}$$

where V denoted the volume of liquid and S the bounding surface. With the aid of (3.1) it is also possible to write the moment in the form

$$\underline{M}_T = \frac{\partial}{\partial t} \int_V (\underline{r} \times \underline{v}) dV + \int_S (\underline{r} \times \underline{v})(\underline{v} \cdot d\underline{S}) + 2\eta \int_V \underline{r} \times (\underline{\Omega} \times \underline{v}) dV + \eta^2 \int_V \underline{\Omega} \times (\underline{\Omega} \times \underline{r}) dV \tag{4.4}$$

with respect to the aeroballistic coordinate system. This formula expresses the fact that the moment is equal to the rate of change of angular momentum.

The fourth term on the right-hand side of (4.4) represents the moment due to solid-body motion and is independent of the velocity field. It is therefore convenient to remove this term and to introduce the quantity $\underline{M}$, representing the (dimensionless) moment induced by the liquid payload, defined by

$$\underline{M} = \frac{\partial}{\partial t}\int_V (\underline{r}\times\underline{v})dV + \int_S (\underline{r}\times\underline{v})(\underline{v}\cdot d\underline{S}) + 2\eta\int_V \underline{r}\times(\underline{\Omega}\times\underline{v})dV \qquad (4.5)$$

The dimensional equivalent of this is given by

$$\underline{M}^* = \rho a^5\omega^2\,\underline{M}\ . \qquad (4.6)$$

The solution being sought is time-independent with respect to the aeroballistic reference frame; this implies that the first term on the right-hand side of (4.5) is identically zero. Moreover, the boundary conditions (3.14) imply that $\underline{v}\cdot d\underline{S} = 0$ on the entire bounding surface. It follows, therefore, that the effective form of (4.5) is

$$\underline{M} = 2\eta\int_V \underline{r}\times(\underline{\Omega}\times\underline{v})dV \qquad (4.7)$$

which is, of course, the contribution from the coriolis force.

We refer the moment to a cartesian coordinate system in the aeroballistic frame; this is the system described at the beginning of Section 3. The components of $\underline{r}$ are (x,y,z), while the components of $\underline{M}$ are denoted

M_x, M_y, M_z. In this terminology M_z represents the despin (roll) moment, M_x the yaw (side) moment and M_y the pitch moment. For the velocity vector $\underline{v}$ it is convenient to write

$$\underline{v} = (-y + u)\hat{\underline{i}} + (x + v)\hat{\underline{j}} + w\hat{\underline{k}} \quad , \tag{4.8}$$

so that (u,v,w) are the components of the deviation from rigid-body rotation. It should be noted that the boundary conditions (3.14) imply the vanishing of u, v and w on all solid boundaries. The components of the angular velocity vector Ω are given by (3.4).

Substituting all the various components into (4.7) we obtain

$$\begin{aligned} M_x &= -2\eta\int_V (yv\sin\theta + zw\sin\theta + zu\cos\theta)dV \\ M_y &= \eta\sigma\pi b + 2\eta\int_V (xv\sin\theta - zv\cos\theta)dV \\ M_z &= 2\eta\int_V (xw\sin\theta + xu\cos\theta + yv\cos\theta)dV \end{aligned} \tag{4.9}$$

where θ is the coning angle and $b = c/a$ is the aspect ratio. It is noteworthy that the rigid-body motion of the liquid contributes only to the pitch moment M_y.

We now establish an exact relationship between the components M_x and M_z. To do this it is convenient to write the first and third of equations (4.9) in the forms

$$\begin{aligned} M_x &= -2\eta(\sin\theta\ I_1 + \sin\vartheta\ I_2 + \cos\theta\ I_3) \\ M_z &= 2\eta(\sin\theta\ K_1 + \cos\theta\ K_2 + \cos\theta\ K_3) \end{aligned} \tag{4.10}$$

where the definitions of the I's and K's are self-evident. Consider first

$$I_1 = \int_V yv\, dV = \iiint yv\,dx\,dy\,dz = \tfrac{1}{2}\iiint v\,d(y^2)\,dx\,dz \quad .$$

Integrating by parts and using the fact that $v = 0$ on the boundaries, we have

$$I_1 = -\tfrac{1}{2}\int_V y^2 \frac{\partial v}{\partial y}\, dV = \tfrac{1}{2}\int_V y^2\left(\frac{\partial u}{\partial x} + \frac{\partial w}{\partial z}\right) dV \quad ,$$

by continuity. Now we can write

$$I_1 = \tfrac{1}{2}\iint y^2 \int \frac{\partial u}{\partial x}\, dx\,dy\,dz + \tfrac{1}{2}\iint y^2 \int \frac{\partial w}{\partial z}\, dz\,dy\,dx$$

and the interior integrals both vanish since $u = 0$ and $w = 0$ on the boundaries. Hence $I_1 = 0$.

By exactly similar procedures we can show that I_2, K_2 and K_3 also vanish. Thus we have the result

$$I_1 = I_2 = K_2 = K_3 = 0 \quad . \tag{4.11}$$

This implies that equations (4.10) reduce to

$$M_x = -2\eta\cos\theta\, I_3 \quad , \qquad M_z = 2\eta\sin\theta\, K_1 \quad . \tag{4.12}$$

Next consider

$$I_3 = \int_V zu\, dV = \iint z \int u\,dx\,dy\,dz = -\int_V zx \frac{\partial u}{\partial x}\, dV \quad ,$$

on integrating by parts and using the condition $u = 0$ on the boundaries.

By continuity

$$I_3 = \int_V xz\left(\frac{\partial v}{\partial y} + \frac{\partial w}{\partial z}\right) dV$$

$$= \iint xz \int \frac{\partial v}{\partial y}\, dydxdz \quad + \quad \iint x \int z \frac{\partial w}{\partial z}\, dzdxdy$$

$$= 0 - \int xw\, dV \quad = \quad -K_1$$

on integrating by parts. Hence we have

$$I_3 + K_1 = 0 \tag{4.13}$$

Applying this result to (4.12) we obtain

$$\sin\theta\, M_x - \cos\theta\, M_z = 0 \quad . \tag{4.14}$$

This is the relationship between M_x and M_z referred to earlier. It should be noted that (4.14) applies to both Newtonian and non-Newtonian fluids, and that its derivation does not depend on any assumptions regarding the parameters of the problem.

Several modifications need to be made to the foregoing discussion when the problem of an infinitely long cylinder is under consideration. In the first place it is no longer possible to refer to the moment on the whole cylinder, since the volume integrals in (4.2) and subsequent equations would be infinite. We can, however, calculate the moment acting on a cylindrical control volume V, with bounding surface S, which encloses a cylinder of fluid of radius a and lenth $2c$. In this case the formulas (4.2)-(4.5) become meaningful when V and S are interpreted in this way.

The mass of liquid inside the control volume is

$$m_L = 2\pi a^2 c\rho \tag{4.15}$$

so that we can conveniently define a liquid-payload-induced moment per unit mass by the formula

$$\underline{m}^* = \underline{M}^*/m_L \quad ; \tag{4.16}$$

this has units $cm^2 \cdot sec^{-2}$. A dimensionless moment per unit mass, denoted $\underline{m}$, can be obtained from this by writing

$$\underline{m}^* = a^2\omega^2\underline{m} \tag{4.17}$$

and it is then easy to show that $\underline{m}$ and $\underline{M}$ are related by the formula

$$\underline{m} = \underline{M}/(2\pi b) \quad . \tag{4.18}$$

The quantities $\underline{m}^*$ and $\underline{m}$ are meaningful for both a finite cylinder and an infinite cylinder, and therefore can be used when results for the two problems are being compared.

The second modification is necessitated by the fact that the flat ends of the control volume are not rigid boundaries, and therefore it is no longer the case that $\underline{v}\cdot d\underline{S} = 0$ on all boundaries. It follows that the effective form of (4.5) is no longer (4.7), but rather

$$\underline{M} = \int_S (\underline{r} \times \underline{v})(\underline{v}\cdot d\underline{S}) + 2\eta\int_V \underline{r} \times (\underline{\Omega} \times \underline{v})dV' \quad , \tag{4.19}$$

where the first term on the right-hand side of this equation may have contributions from the flat ends. Precisely what these contributions are

will become apparent in the next Section where the calculations for the infinitely long cylinder are presented.

Finally, we do not expect the relationship (4.14) to hold in the infinite cylinder case. Not only are the moments affected by the additional term in (4.19), but also the identities (4.11) and (4.13) cannot be established. This is because the proofs of these depend on the fact that the components u,v,w are all zero on all boundaries; but this is no longer true on the flat ends of the control volume. Consequently the proofs break down and the results do not apply. In the next Section we shall discuss the relationship between M_x and M_z as it emerges from our solution.

5. INFINITELY LONG CYLINDER

In this Section and the next we shall be considering the special, and obviously unrealistic, case of an infinitely long cylinder. This problem was analyzed in considerable detail by Herbert (1985) for the Newtonian liquid; we shall adapt Herbert's procedures to the non-Newtonian liquid, and shall indicate similarities and dissimilarities as appropriate.

There are two reasons for pursuing the infinite-cylinder problem. The first is that it is possible to obtain an approximate analytic solution in the case that the spin ratio (Ω/ω) is small, which does indeed apply in most situations of practical interest. The second is that the results obtained should be relevant to the case of a cylinder which is finite but of large aspect ratio. As indicated in the previous Section, however, and shown further below, some reservations need to be made in interpreting infinite-cylinder results for the moments when one has the finite cylinder in mind.

The governing equations are (3.1)-(3.2), together with one of the constitutive relations listed in Section 3. The boundary conditions (3.14) are modified, however, for infinite aspect ratio to read

$$\underline{v} = \hat{\underline{\phi}} \quad \text{on } r = 1$$
$$\underline{v} \text{ bounded as } r \to 0 \tag{5.1}$$

It is assumed that the spin ratio η is small, and a solution is developed through a regular perturbation procedure.

We expand the field quantities appearing in the governing equations in power series of the following forms,

$$\begin{aligned} \underline{v} &= \underline{v}^{(0)} + \eta\underline{v}^{(1)} + \eta^2\underline{v}^{(2)} + \cdots \\ \underline{\tau} &= \underline{\tau}^{(0)} + \eta\underline{\tau}^{(1)} + \eta^2\underline{\tau}^{(2)} + \cdots \\ p &= p^{(0)} + \eta p^{(1)} + \eta^2 p^{(2)} + \cdots \end{aligned} \tag{5.2}$$

Associated with these will be similar expansions of the strain-rate and vorticity tensors,

$$\begin{aligned} \dot{\underline{\gamma}} &= \dot{\underline{\gamma}}^{(0)} + \eta\dot{\underline{\gamma}}^{(1)} + \eta^2\dot{\underline{\gamma}}^{(2)} + \cdots \\ \underline{\omega} &= \underline{\omega}^{(0)} + \eta\underline{\omega}^{(1)} + \eta^2\underline{\omega}^{(2)} + \cdots \end{aligned} \tag{5.3}$$

These representations are substituted into the governing equations (3.1) -(3.2), the boundary conditions (5.1), and the appropriate constitutive equations, and the terms corresponding to like powers of η are equated. This results in a sequence of boundary-value problems which are in principle amenable to analytic solution.

It is easy to show that the leading-order solution, corresponding to $\eta = 0$, is simply the rigid-body motion of the liquid, and this is independent of the particular constitutive equation chosen. In fact we have that

$$\begin{aligned} &\underline{v}^{(0)} = r\hat{\underline{\phi}}, \quad \underline{\tau}^{(0)} = 0, \quad p^{(0)} = \tfrac{1}{2} r^2 , \\ &\dot{\underline{\gamma}}^{(0)} = 0, \quad \underline{\omega}^{(0)} = \hat{\underline{r}}\,\hat{\underline{\phi}} - \hat{\underline{\phi}}\,\hat{\underline{r}} \quad . \end{aligned} \tag{5.4}$$

It should be noted that the strain-rate tensor is zero, while the vorticity tensor has components appropriate to rigid-body rotation.

At the next order, corresponding to $O(\eta)$, equations (3.1)-(3.2) become

$$\underline{v}_t^{(1)} + \underline{v}_\phi^{(1)} + (\underline{v}^{(1)}\cdot\nabla)r\underline{\hat{\phi}} + 2\underline{\Omega}\times r\underline{\hat{\phi}} = -\nabla p^{(1)} + \frac{1}{Re}\nabla\cdot\underline{\tau}^{(1)} \tag{5.5}$$

$$\nabla\cdot\underline{v}^{(1)} = 0 \tag{5.6}$$

while the boundary conditions (4.1) become

$$\begin{aligned} &\underline{v}^{(1)} = 0 \quad \text{on } r = 1 \\ &\underline{v}^{(1)} \text{ bounded as } r \to 0 \ . \end{aligned} \tag{5.7}$$

The appropriate approximation for each of the constitutive relations discussed in the preceding Section can easily be written down. From the Carreau model (3.6) we obtain

$$\underline{\tau}^{(1)} = 2\dot{\underline{\gamma}}^{(1)} \tag{5.8}$$

which is the same as for a Newtonian liquid. This is due to the fact that $\dot{\gamma}$ appears in the denominator of (3.6) in quadratic form, and therefore the nonlinearity makes no contribution at this order.

For the second-order fluid model (3.8) we obtain

$$\underline{\tau}^{(1)} = 2\dot{\underline{\gamma}}^{(1)} - 2We(\dot{\underline{\gamma}}_t^{(1)} + \dot{\underline{\gamma}}_\phi^{(1)} + \underline{\omega}^{(0)}\cdot\dot{\underline{\gamma}}^{(1)} - \dot{\underline{\gamma}}^{(1)}\cdot\underline{\omega}^{(0)}) \tag{5.9}$$

which, it should be noted, does not contain either of the parameters a or κ. The form of the CEF equation (3.11) depends on the functions Φ_1, Φ_2, Φ_3 but if, as is usually the case, these are quadratic in $\dot{\gamma}$, then the reduced form of the CEF equation is also (5.9), the same as that of the second-order fluid equation.

The differential model (3.12) becomes

$$\underline{\tau}^{(1)} + We(\underline{\tau}_t^{(1)} + \underline{\tau}_\phi^{(1)} + \underline{\omega}^{(0)}\cdot\underline{\tau}^{(1)} - \underline{\tau}^{(1)}\cdot\underline{\omega}^{(0)})$$

$$= 2\dot{\underline{\gamma}}^{(1)} + 2\epsilon We(\dot{\underline{\gamma}}_t^{(1)} + \dot{\underline{\gamma}}_\phi^{(1)} + \underline{\omega}^{(0)}\cdot\underline{\gamma}^{(1)} - \underline{\gamma}^{(1)}\cdot\underline{\omega}^{(0)}) \quad . \tag{5.10}$$

It should be observed that the parameter a, which determines the extent of shear thinning in the model, is absent from (5.10); in this problem upper convected, lower convected and corotational models all reduce to the same form in this approximation.

The problem determined by equations (5.5)-(5.6) and one of (5.8), (5.9) or (5.10) has a time-independent solution with the velocity vector being of the form

$$\underline{v}^{(1)} = [\ 0,\ 0,\ \ w(r,\phi)\ ] \ . \tag{5.11}$$

The flow is purely axial and depends only on the plane coordinates r,ϕ. With this flow field the strain-rate and stress tensors are respectively,

$$\dot{\underline{\gamma}}^{(1)} = \frac{1}{2}\begin{pmatrix} 0 & 0 & w_r \\ 0 & 0 & \frac{1}{r}w_\phi \\ w_r & \frac{1}{r}w_\phi & 0 \end{pmatrix} \qquad \underline{\tau}^{(1)} = \begin{pmatrix} 0 & 0 & \tau_{13} \\ 0 & 0 & \tau_{23} \\ \tau_{13} & \tau_{23} & 0 \end{pmatrix} \ . \tag{5.12}$$

Equations (5.5) and (5.6) now simplify to

$$p^{(1)} = \sqrt{1-\sigma^2}\cdot r^2 \tag{5.13}$$

and the equation,

$$w_\phi - 2\sigma r\cos\phi = \frac{1}{Re}\left[\tfrac{1}{r}(r\tau_{13})_r + \tfrac{1}{r}\tau_{23,\phi}\right] \tag{5.14}$$

with the boundary conditions

$$w = 0 \quad \text{on } r = 1, \qquad w \text{ bounded at } r = 0 \ . \tag{5.15}$$

In the case of the (Newtonian) constitutive relation (5.8) we find that

$$\tau_{13} = w_r, \qquad \tau_{23} = \tfrac{1}{r} w_\phi \tag{5.16}$$

so that (5.14) becomes

$$w_\phi - 2\sigma r \cos\phi = \frac{1}{\mathrm{Re}} \nabla^2 w \tag{5.17}$$

where ∇^2 is the two-dimensional Laplacian operator in the r,ϕ-plane. This is the equation solved by Herbert (1985).

In the case of the second-order fluid relation (5.9) we find that

$$\tau_{13} = (w - \mathrm{We}\, w_\phi)_r \ , \qquad \tau_{23} = \tfrac{1}{r}(w - \mathrm{We}\, w_\phi)_\phi \tag{5.18}$$

which reduces (5.14) to the equation

$$w_\phi - 2\sigma r \cos\phi = \frac{1}{\mathrm{Re}} \nabla^2 (w - \mathrm{We}\, w_\phi) \ . \tag{5.19}$$

In the case of the differential model (5.10) we obtain

$$\begin{aligned} \tau_{13} + \mathrm{We}\, \tau_{13,\phi} &= (w + \epsilon \mathrm{We}\, w_\phi)_r \\ \tau_{23} + \mathrm{We}\, \tau_{23,\phi} &= \tfrac{1}{r}(w + \epsilon \mathrm{We}\, w_\phi)_\phi \end{aligned} \tag{5.20}$$

Although these equations can be solved for τ_{13} and τ_{23}, and the solution substituted into (5.14), we shall refrain from doing so at this point since the subsequent development provides an easier way of achieving the desired result.

Following Herbert (1985) we solve the problem by writing

$$\begin{aligned} w &= 2\sigma\,[f(r)\cos\phi + g(r)\sin\phi] \\ &= 2\sigma\cdot\text{Real}\,[h(r)e^{-i\phi}] \end{aligned} \tag{5.21}$$

where $h = f + ig$. Equation (5.17) becomes

$$r^2h'' + rh' - (1 - i\text{Re}r^2)h = -\text{Re}r^3 \quad . \tag{5.22}$$

Equation (5.19) becomes

$$r^2h'' + rh' - \left(1 - \frac{i\text{Re}r^2}{1+i\text{We}}\right)h = \frac{-\text{Re}r^3}{1+i\text{We}} \quad . \tag{5.23}$$

In the third, differential case we find the solutions of (5.20) to be

$$\begin{aligned} \tau_{13} &= 2\sigma\cdot\text{Real}\left(\frac{(1-i\epsilon\text{We})h'\,e^{-i\phi}}{1 - i\text{We}}\right) \\ \tau_{23} &= 2\sigma\cdot\text{Real}\left(\frac{-i(1-i\epsilon\text{We})he^{-i\phi}}{r(1 - i\text{We})}\right) \end{aligned} \tag{5.24}$$

whereupon the appropriate equation is found to be

$$r^2h'' + rh' - \left(1 - \frac{i\text{Re}(1-i\text{We})r^2}{1 - i\epsilon\text{We}}\right)h = \frac{-\text{Re}(1-i\text{We})r^3}{1 - i\epsilon\text{We}} \quad . \tag{5.25}$$

The boundary conditions are

$$h = 0 \text{ at } r = 1, \qquad h \text{ bounded at } r = 0 \quad . \tag{5.26}$$

We see that equations (5.22), (5.23) and (5.25) all have the same structure. In fact they can all be written in the single unified form

$$r^2h'' + rh' - (1 - iSr^2)h = -Sr^3 \tag{5.27}$$

where

$$S = \mathrm{Re} \qquad \text{(Newtonian and power-law models)} \tag{5.28}$$

$$S = \frac{\mathrm{Re}}{1+i\mathrm{We}} \qquad \text{(second-order fluid model)} \tag{5.29}$$

$$S = \frac{(1-i\mathrm{We})\mathrm{Re}}{1-i\epsilon\mathrm{We}} \qquad \text{(differential model)} \quad . \tag{5.30}$$

It is noteworthy that for the second-order-fluid and differential models the parameter S has the form of a complex Reynolds number. Thus in these two cases it seems that the non-Newtonian effects are in a sense representable by a complex viscosity; this occurs in other flow configurations of viscoelastic fluids, for example in time-dependent flows where stress relaxation is important.

The solution of (5.27) which satisfies the boundary conditions (5.26) is

$$h = i\left\{ r - \frac{I_1(qr)}{I_1(q)} \right\} \tag{5.31}$$

where

$$q^2 = -iS \tag{5.32}$$

and I_1 is the modified Bessel function of order unity. The flow field can be completely determined by a simple computation of the Bessel functions.

Before proceeding to discuss the moment acting on the cylinder, we note that approximate forms of (5.31) for small and large $|S|$ are easily found.

When $|S| \ll 1$ we apply standard formulas for series expansions of the Bessel functions to obtain

$$h = \frac{S}{8}(r - r^3) + \frac{iS^2}{192}(2r - 3r^3 + r^5) + O(S^3) \quad . \tag{5.33}$$

In the case of a Newtonian or power-law fluid we have that S=Re, so that $|S| \ll 1$ corresponds simply to a small Reynolds number approximation. The separation of (5.33) into its real and imaginary parts ($h = f + ig$) gives

$$f = \frac{\mathrm{Re}}{8}(r - r^3) \ , \qquad g = \frac{\mathrm{Re}^2}{192}(2r - 3r^3 + r^5) \tag{5.34}$$

to a leading approximation, in agreement with Herbert (1985).

For the second-order fluid (5.29) the condition $|S| \ll 1$ is achieved when $\mathrm{Re} \ll 1$. It can also be achieved for very large We, but this is an anomalous case since the second-order fluid model is known to be invalid at large Weissenberg number. The real and imaginary parts of (5.33) are found to be

$$\begin{aligned} f &= \frac{\mathrm{Re}}{8(1+\mathrm{We}^2)}(r - r^3) + \frac{\mathrm{Re}^2\mathrm{We}}{96(1+\mathrm{We}^2)^2}(2r - 3r^3 + r^5) \\ g &= \frac{-\mathrm{ReWe}}{8(1+\mathrm{We}^2)}(r - r^3) + \frac{\mathrm{Re}^2(1-\mathrm{We}^2)}{192(1+\mathrm{We}^2)^2}(2r - 3r^3 + r^5) \quad ; \end{aligned} \tag{5.35}$$

this is significantly different from (5.34) in that the component g now has a term proportional to Re, whereas there is no such term in equation (5.34).

For the differential model (5.30) the condition $|S| \ll 1$ is again achieved when $Re \ll 1$. Provided $\epsilon \neq 0$ the condition $Re \ll 1$ implies that $|S| \ll 1$ for the whole range of values of We. When $\epsilon = 0$, however, it is clearly necessary to impose the additional requirement $WeRe \ll 1$ to ensure that $|S| \ll 1$. In this case (5.33) gives

$$f = \frac{Re(1+\epsilon We^2)}{8(1+\epsilon^2 We^2)}(r - r^3) + \frac{Re^2 We(1-\epsilon)(1+\epsilon We^2)}{96(1+\epsilon^2 We^2)^2}(2r - 3r^3 + r^5) \qquad (5.36)$$

$$g = \frac{-(1-\epsilon)ReWe}{8(1+\epsilon^2 We^2)}(r - r^3) + \frac{Re^2[(1+\epsilon We^2)^2-(1-\epsilon)^2 We^2]}{192(1+\epsilon^2 We^2)^2}(2r - 3r^3 + r^5) \quad .$$

Again there is a term proportional to the Reynolds number in the component g.

In all three cases (5.28)-(5.30) the limit $|S| \to \infty$ is equivalent to $Re \to \infty$, irrespective of Weissenberg number. The effects of elasticity disappear in this limit and all the cases are effectively Newtonian. Asymptotic results in the limit $Re \to \infty$ have been provided by Herbert (1985).

We proceed now to calculate the moment in the present configuration. We take a control volume V with bounding surface S which coincides with a cylinder of liquid of dimensionless length $2b$ and dimensionless radius 1, and whose center coincides with the origin of the coordinate system. As shown in Section 4, equation (4.19), the liquid-induced moment acting on this control volume has the form

$$\underline{M} = \underline{M}_S + \underline{M}_V \qquad (5.37)$$

where

$$\underline{M}_S = \int_S (\underline{r} \times \underline{v})(\underline{v} \cdot d\underline{S}) \quad , \qquad \underline{M}_V = 2\eta \int_V \underline{r} \times (\underline{\Omega} \times \underline{v}) dV \quad . \tag{5.38}$$

As indicated previously, the contribution $\underline{M}_S$ arises entirely from the fact that the boundaries at the flat ends of the control volume are not rigid.

We shall compute $\underline{M}_S$ and $\underline{M}_V$ separately for the case of small spin ratio. First, we write

$$\underline{M}_S = \underline{M}_S^{(0)} + \eta \underline{M}_S^{(1)} + \eta^2 \underline{M}_S^{(2)} + \cdots \tag{5.39}$$

Then, substituting (5.2) and (5.39), and equating coefficients of like powers of η, we obtain

$$\underline{M}_S^{(0)} = \int_S (\underline{r} \times \underline{v}^{(0)})(\underline{v}^{(0)} \cdot d\underline{S}) \tag{5.40}$$

$$\underline{M}_S^{(1)} = \int_S (\underline{r} \times \underline{v}^{(0)})(\underline{v}^{(1)} \cdot d\underline{S}) + \int_S (\underline{r} \times \underline{v}^{(1)})(\underline{v}^{(0)} \cdot d\underline{S}) \tag{5.41}$$

$$\underline{M}_S^{(2)} = \int_S (\underline{r} \times \underline{v}^{(0)})(\underline{v}^{(2)} \cdot d\underline{S}) + \int_S (\underline{r} \times \underline{v}^{(1)})(\underline{v}^{(1)} \cdot d\underline{S}) + \int_S (\underline{r} \times \underline{v}^{(2)})(\underline{v}^{(0)} \cdot d\underline{S}) \tag{5.42}$$

for the first three terms in the series for $\underline{M}_S$.

Now $\underline{v}^{(0)}$ is given by (5.4), and it is obvious that $\underline{v}^{(0)} \cdot d\underline{S}$ vanishes everywhere on S. Hence (5.40) gives

$$\underline{M}_S^{(0)} = 0 \quad . \tag{5.43}$$

Next consider (5.41). For the reason just stated the second integral on the right-hand side of (5.41) is identically zero, while the first integral reduces to an integral over the two flat ends, with (5.11) giving $\underline{v}^{(1)} \cdot d\underline{S} = \pm wrdrd\phi$ on $z = \pm b$ respectively. We then obtain

$$\underline{M}_S^{(1)} = -2b\iint r^2 w\, \hat{\underline{r}}\, drd\phi \quad , \tag{5.44}$$

the integration being over $0 < r < 1$, $0 < \phi < 2\pi$. We express the moment in terms of its cartesian components by using the transformations

$$\hat{\underline{r}} = \cos\phi\, \hat{\underline{i}} + \sin\phi\, \hat{\underline{j}} \quad , \qquad \hat{\underline{\phi}} = -\sin\phi\, \hat{\underline{i}} + \cos\phi\, \hat{\underline{j}} \tag{5.45}$$

and the representation (5.21) for w. Then we obtain from (5.44) non-zero x and y components,

$$M_{s,x}^{(1)} = -4\pi\sigma b\int_0^1 r^2 f(r)dr \tag{5.46}$$

$$M_{s,y}^{(1)} = -4\pi\sigma b\int_0^1 r^2 g(r)dr \quad , \tag{5.47}$$

and the z-component is found to be identically zero.

It is easy to show, finally, that

$$\underline{M}_S^{(2)} = 0 \tag{5.48}$$

for the following reasons. Although $\underline{v}^{(2)}$ has not been calculated explicitly, it can be demonstrated with little difficulty that $\underline{v}^{(2)}$ has no component in the z-direction. Hence $\underline{v}^{(2)} \cdot d\underline{S} = 0$ on the surface, and so the first integral on the right-hand side of (5.42) vanishes. The third

integral vanishes because $\underline{v}^{(0)} \cdot d\underline{S} = 0$ on the surface. The second integral can be shown to vanish because of symmetry considerations.

Summarizing these results we have that

$$\underline{M}_S = \eta \left(-4\pi\sigma b \int_0^1 r^2 f(r) dr \, \hat{\underline{i}} - 4\pi\sigma b \int_0^1 r^2 g(r) dr \, \hat{\underline{j}} \right) + O(\eta^3) \quad . \tag{5.49}$$

We now turn to the contribution $\underline{M}_V$, which arises from the coriolis force. Writing

$$\underline{M}_V = \underline{M}_V^{(0)} + \eta \underline{M}_V^{(1)} + \eta^2 \underline{M}_V^{(2)} + \cdots \tag{5.50}$$

and substituting into (5.38), we obtain

$$\underline{M}_V^{(0)} = 0 \tag{5.51}$$

$$\underline{M}_V^{(1)} = 2 \int_V \underline{r} \times (\underline{\Omega} \times \underline{v}^{(0)}) dV \tag{5.52}$$

$$\underline{M}_V^{(2)} = 2 \int_V \underline{r} \times (\underline{\Omega} \times \underline{v}^{(1)}) dV \quad . \tag{5.53}$$

Using (3.15) and (5.4) we easily show that

$$\underline{M}_V^{(1)} = \pi b \sigma \, \hat{\underline{j}} \tag{5.54}$$

and using (3.15), (5.11) and (5.21) we find

$$\underline{M}_V^{(2)} = 8\pi b \sigma^2 \int_0^1 r^2 f(r) dr \, \hat{\underline{k}} \quad . \tag{5.55}$$

Thus we have that

$$\underline{M}_V = \eta \cdot \pi b \sigma \, \hat{\underline{j}} + \eta^2 \cdot 8\pi b \sigma^2 \int_0^1 r^2 f(r) dr \, \hat{\underline{k}} + O(\eta^3) \quad . \tag{5.56}$$

Combining (5.49) and (5.56) we obtain

$$\underline{M} = \eta\left(-4\pi\sigma b\int_0^1 r^2 f(r)\,dr\right)\hat{\underline{i}} + \eta\left(\pi b\sigma - 4\pi b\sigma\int_0^1 r^2 g(r)\,dr\right)\hat{\underline{j}} \qquad (5.57)$$

$$+ \eta^2\cdot 8\pi b\sigma^2\int_0^1 r^2 f(r)\,dr\,\hat{\underline{k}} + O(\eta^3) \quad .$$

This can be written in an alternative, more convenient, form. By integrating equation (5.27) and using the boundary conditions (5.26) we find that

$$\int_0^1 r^2 h(r)\,dr = \frac{ih'(1)}{S} + \frac{i}{4} \quad . \qquad (5.58)$$

We take the real and imaginary parts of this expression and substitute into (5.57), which then becomes

$$\underline{M} = \eta\cdot -4\pi\sigma b\ \mathrm{Real}\left(\frac{ih'(1)}{S}\right)\hat{\underline{i}} + \eta\cdot -4\pi b\sigma\ \mathrm{Imag}\left(\frac{ih'(1)}{S}\right)\hat{\underline{j}} \qquad (5.59)$$

$$+ \eta^2\cdot 8\pi b\sigma^2\ \mathrm{Real}\left(\frac{ih'(1)}{S}\right)\hat{\underline{k}} + O(\eta^3) \quad .$$

If the components of $\underline{M}$ are denoted by M_x, M_y, M_z, we see from (5.59) that

$$M_z = -2\eta\sigma M_x \qquad (5.60)$$

which agrees with the result obtained by Herbert (1985) for the Newtonian fluid.

It is important to note that the despin moment M_z, which derives from the moment of the coriolis force $\underline{M}_V$, can give a reasonable approximation to the corresponding quantity for a cylinder of finite length (with large aspect ratio). The other two components M_x, M_y given by (5.59) are

entirely spurious as far as the finite-cylinder situation is concerned, since they both contain contributions from surface integrals over the flat ends. Similarly the relation (5.60), which differs from (4.14), is also spurious.

From (5.59), therefore, we note for future reference that the despin moment is given by the expression

$$M_z = \eta^2 \cdot 8\pi b\sigma^2 \,\mathrm{Real}\left(\frac{ih'(1)}{S}\right) \tag{5.61}$$

to leading order.

In the next Section we give numerical results based on the calculations presented above.

6. INFINITELY LONG CYLINDER: RESULTS

The purpose of the calculations reported in this Section was to demonstrate how the inclusion of non-Newtonian effects modified the flow field and the despin moment as computed by Herbert (1985). We were interested primarily in sensitivity to departure from Newtonian behavior rather than determining even an approximation to the solution that was applicable to the case of a closed cylinder of finite length. The most that can be expected of the present calculation would be some qualitative insight into the consequences of including viscoelasticity in the model.

The results herein are based on equation (5.31), which gives the components f and g of the axial velocity in complex form, and on equation (5.61), which gives the despin moment at leading order. The computation of the Bessel functions involved is straight-forward, and we have used a combination of the series and asymptotic formulas for these functions to cover the required parameter range.

We note first that, according to equation (5.28), the power-law model predicts the same velocity field and despin moment as does the Newtonian model. It should be emphasized that this prediction is entirely a consequence of the linearizing expansions (5.2) and (5.3), and would fail to hold when these expansions break down. This question will be discussed in more detail subsequently.

For the differential model, with "complex viscosity" S given by formula (5.30), we show in Figures 2 and 3 respectively the variation of f and g

with radius at a Reynolds number Re = 15. Included in these Figures are the appropriate Newtonian curves (We = 0) which are identical with those presented by Herbert (1985). The three non-Newtonian cases shown in these Figures correspond to various values of Deborah number De and retardation parameter ϵ, namely, De = 0.1, ϵ = 0.1; De = 0.2, ϵ = 0.1; De = 0.2, ϵ = 0.2, respectively. It is clear that the velocity fields are considerably distorted by comparison with the Newtonian case, particularly for the component f which, from (5.21), corresponds to the flow in the plane ϕ = 0. There is here a backflow near the cylinder center and the appearance of a boundary layer near the wall.

Figures 4 and 5 show the variation of the same quantities, f and g, with radius for the same parameter values, but at Reynolds number Re = 50. Again the distortions in the velocity fields for the viscoelastic cases are self-evident. In a very broad sense the non-Newtonian velocity fields at Re = 15 are comparable with the Newtonian velocity fields at Re = 50, which is consistent with the shear-thinning nature of the viscoelastic model.

The despin moment as a function of Reynolds number for this model is shown in Figure 6. The quantity actually plotted in this diagram is, for convenience, denoted M and defined by

$$M = \frac{M_z}{\eta^2 \cdot 8\pi b\sigma^2} = \text{Real}\left[\frac{ih'(1)}{S}\right] \tag{6.1}$$

from equation (5.61). It is therefore possible to compute the despin moment on a control volume of dimensionless length $2b$ as well as the despin moment per unit length. The important features observed from Figure

6 are, firstly, at low Reynolds numbers the despin moment is larger in the viscoelastic cases than in the Newtonian case; secondly, at large Reynolds numbers the effect of viscoelasticity is to reduce the despin moment by comparison with the Newtonian case; and thirdly, the maximum despin moment occurs at a lower Reynolds number (Re ≈ 5-10) for the viscoelastic liquids than for the Newtonian liquid (Re ≈ 15). These suggest that there can be quite significant non-Newtonian effects in the precise low Reynolds number regime where the high viscosity instability is of practical concern.

It is interesting to compare these results with their equivalents for the second-order fluid, for which S is given by (5.29). In Figures 7-10 we show the variation of f and g with radius at Reynolds numbers Re = 15 (Figures 7 and 8) and Re = 50 (Figures 9 and 10). In addition to the Newtonian curves (included for purposes of comparison) we show the curves for values of Deborah number De = 0.01 and De = 0.1. It is clear that the distortions due to non-Newtonian effects are very different from those in the differential model. Figure 11 shows the quantity M, defined by (6.1), as a function of Reynolds number for the same parameter values De = 0.01 and De = 0.1. Again the differences between the differential model and the second-order fluid model are striking. In the latter case, as shown in Figure 11, although the moment increases due to non-Newtonian effects, the Reynolds number at which it attains its peak is greater then in the Newtonian case.

These results highlight the importance of a proper representation of non-Newtonian behavior through the choice of a constitutive model des-

cribing the fluid motion of interest. In part the differences between the moments shown in Figures 6 and 11 can be understood from the following argument. The value of the moment is effectively determined by the quantity S and how the Bessel functions vary with S. For the second-order fluid, from (5.29),

$$|S| = \frac{\mathrm{Re}}{|1 + i\mathrm{We}|} < \mathrm{Re} \tag{6.2}$$

while for the differential model (5.30)

$$|S| = \mathrm{Re}\,\frac{|1 - i\mathrm{We}|}{|1 - i\epsilon\mathrm{We}|} > \mathrm{Re} \tag{6.3}$$

for any value of the Weissenberg number. Thus if we tentatively take the view that $|S|$ is an effective Reynolds number, we see that the Reynolds number is reduced (viscosity is increased: shear thickening) for the second-order fluid, while the Reynolds number is increased (viscosity is decreased: shear thinning) for the differential model. The general shapes of the curves in Figures 6 and 11 are consistent with these notions.

7. FINITE ELEMENT METHOD

The problem as posed in Section 3 was solved numerically by a finite element method, using the software package FIDAP (Fluid Dynamics Analysis Package). FIDAP is a commercial, general purpose code for the solution of incompressible fluid flow problems governed by the Navier-Stokes equations, and including non-isothermal effects. The code applies to both transient and steady flows, and can handle three-dimensional problems. It has the capability of addressing flows of non-Newtonian fluids.

In the present work the problem was posed in the aeroballistic reference frame discussed previously. In this frame the problem is three-dimensional and a steady state solution is required. No thermal effects are considered.

The essential features of the finite element method as incorporated in FIDAP are as follows. The domain of interest, the interior of the cylinder, is divided into a number of geometrically simple elements, thereby generating the finite element mesh. Since the code FIDAP works in cartesian coordinate systems, the elements are straight-sided even though a portion of the cylinder boundary is curved. The number of elements used is a crucial factor in determining the running time of the program, and this consideration has to be balanced against accuracy requirements. The finer the mesh, the greater the accuracy and, simultaneously, the cost; and conversely, coarsening the mesh decreases both accuracy and cost. The principal criterion in deciding on the mesh is that the associated approximations should be sufficient to resolve the flow field everywhere. This means, for example, that the mesh needs to be quite fine in

regions where boundary layers occur so that large gradients of the velocity field can be appropriately taken into account. Thus, flows at low Reynolds numbers can generally be handled with a fairly coarse mesh, while high Reynolds number flows require a much finer mesh.

In the present project, after considerable experimentation, a mesh was designed that was adequate for low and moderate Reynolds numbers, over the range $0 < Re < 2500$ approximately. At the lower end of the Reynolds number range a coarser mesh would no doubt have sufficed, but it was decided to retain the rather fine mesh throughout the computations in the interests of obtaining better accuracy. It should be pointed out that the Reynolds number referred to here is the zero-shear-rate Reynolds number; in the non-Newtonian situation the actual Reynolds number is considerably higher due to shear thinning.

The working mesh had 2240 elements, which were 8-node bricks, and 2541 nodes. The mesh is shown in Figure 12.

In the finite element method the velocity vector is approximated on each element by a simple polynomial function. In the present case the velocities were approximated by trilinear interpolation functions, while the pressure was represented by a piecewise constant discontinuous function. The Galerkin method of weighted residuals reduces the Navier-Stokes and continuity equations, together with the boundary conditions, to a large system of nonlinear algebraic equations which then need to be solved by an appropriate technique. The solution procedure used here was a quasi-Newton method, which is an iterative method of Newton type involving updating of the iteration matrix.

The procedure adopted in solving the problem with FIDAP can be summarized as follows:

1. An input file was prepared which included,

   (a) the specification of the mesh;

   (b) the specification of the boundary conditions, namely that the container is in rigid body rotation in the aeroballistic frame, by a call to a subroutine that contains the boundary conditions information;

   (c) the specification of the solution procedure, chosen from among several options available in FIDAP;

   (d) the specification of the non-Newtonian properties of the liquid; this will be described in more detail in the next Section.

2. The program FIDAP was run on a Hewlett Packard 9000 computer. it was found that only 3-4 iterations of the quasi-Newton method were required to achieve convergence, and the typical run time on this machine was about 12 hours of cpu time. The first run was at a low Reynolds number, and subsequent runs at higher Reynolds numbers were performed by restarting from the solution obtained in the previous run.

3. The output was sent to a post-processor file from which graphical information concerning the flow field could be extracted.

4. A subroutine was used to compute the three components of the moment in accordance with the formula (4.9).

In the next Section we detail the results of the calculations.

8. COMPUTATIONS

To begin with, in order to test the code and the viability of the mesh, we performed a sequence of computations for a Newtonian liquid over a range of Reynolds numbers. The aspect ratio of the cylinder in this case was $b = 4.368$, the coning angle was $\theta = 20°$, and the spin ratio was $\eta = 1/6$. These quantities were held fixed and the Reynolds number was varied over the range Re = 10 to Re = 1000. Figure 13 shows the variation of the roll moment M_z with Reynolds number over this range. It should be noted that the quantity M_z plotted here and in all subsequent graphs is the dimensionless roll moment as defined by equation (4.9). In accordance with formula (4.6) the conversion to dimensional form is effected by the transformation

$$M_z^* = \rho a^5 \omega^2 M_z \quad . \tag{8.1}$$

It can be seen from Figure 13 that the maximum roll moment occurs at a Reynolds number approximately equal to 40. This is larger than the value predicted by Herbert (1985) but the latter, of course, applied to the case of an infinite cylinder. The general shape of the curve, however, is consistent with that obtained from the infinite cylinder approximation as shown, for example, in Figure 6.

The detailed values of the three components of the moment are shown in Table 1. The Reynolds numbers listed in the first column are those actually used in stepping the solutions by restarting from the solution of the previous run. The quantities M_x, M_z are the dimensionless values defined by equation (4.9), while the quantity $\tilde{M}_y$ is the pitching moment due to deviation from solid body rotation, namely

$$\tilde{M}_y = M_y - \eta\omega\pi b \quad . \tag{8.2}$$

In column 5 of Table 1 we have written the ratio M_z/M_x. According to the calculation presented in Section 4 this ratio should exactly equal $\tan\theta = .3640$ when $\theta = 20°$. The closeness of the number in column 5 to this value is one good indication of the accuracy of the computation.

Typical flow fields from this computation are shown in Figures 14-18. Figures 14(a),(b),(c) show the velocity vector in the transverse plane defined by $z = 4.0$ for values of the Reynolds number Re = 20, 300, 1000 respectively, while Figures 15(a),(b),(c) show the equivalent velocity vectors at the same respective Reynolds numbers in the plane $z = -4.0$. These two planes, it should be recalled, are quite close to the cylinder ends. Figures 16(a),(b),(c) illustrate the contours of constant axial velocity in the plane $z = 4.0$. The legends in the Figures show the regions of upflow and downflow. An especially interesting feature of these diagrams is the development of the boundary layers at the wall of the cylinder; the boundary layers are already in evidence when Re = 300 and are quite strong when Re = 1000. Figures 17(a),(b),(c) show the velocity vector in the axial cross-section of the cylinder lying in the plane formed by the vectors ω and Ω, that is, the plane $\phi = 0$, while Figures 18(a),(b),(c) depict the same velocity field in the orthogonal axial plane, namely $\phi = \pi/2$. These Figures clearly show the formation of two regions of strong vortex-like motion as the Reynolds number increases.

Next we performed the calculations for two non-Newtonian liquids of interest to CRDC. The properties of these liquids were presented in the

form of experimental data in which the variation of viscosity with shear rate had been measured. Some data on the variation of normal stress with shear rate was also available, but only for a very limited range of shear rates. A constitutive relation, for example of differential type, was not known for either of these liquids, nor was it possible to construct one on the basis of the available data. The measurements, moreover, were understood to have been performed in simple shearing experiments, in which the nature of the flow was very different from that in the spinning and nutating cylinder.

In the absence of appropriate data for the liquids under the flow conditions prevailing in the present problem, it was decided to simulate the non-Newtonian effects by entering a shear-rate-dependent viscosity function extrapolated from the data provided. This data is shown in Table 2. One of the liquids, henceforth referred to as Liquid 1, was a relatively low viscosity liquid, with a zero-shear-rate value of about 8 poise, while the other, Liquid 2, was a high viscosity liquid with $\mu_0 \approx 1300$ poise.

The calculations were performed for a cylinder of aspect ratio $b = 4.50$ and for various values of η, β and Re. This aspect ratio applied to a test fixture having radius 5.54 cm and length 49.84 cm. Before presenting the results of the computations, we note that the Reynolds number for Liquid 1 corresponding to the given zero-shear-rate viscosity and a spin rate of 4000 rpm is approximately Re = 1700, and increases to Re = 2500 for spin rate of 6000 rpm. For Liquid 1, therefore, the calculations are close to the limits of the chosen mesh. For Liquid 2, the

corresponding (Newtonian) Reynolds numbers range from Re ≈ 10 for ω = 4000 r.p.m. to Re ≈ 15 for ω = 6000 r.p.m.

Figures 19 and 20 relate to Liquid 1. Figure 19 shows the variation of dimensionless roll moment M_z with Reynolds number in the case Ω = 400 rpm, ω = 4000 rpm, θ = 20°. The solid curve in this Figure depicts the behavior for the given non-Newtonian Liquid 1, while the broken curve represents the behavior of the "equivalent" Newtonian liquid, that is, the Newtonian liquid having viscosity equal to the zero-shear-rate viscosity of Liquid 1. Figure 20 shows a repeat of these calculations for ω = 4800 rpm, other quantities remaining the same. We see that at these relatively high Reynolds numbers the non-Newtonian liquid experiences a smaller despin moment than its Newtonian counterpart. This result is consistent with the predictions of the analytic approximation for a viscoelastic fluid as shown in Figure 6.

Figures 21 and 22 present the same type of information for Liquid 2. Figure 21 shows the variation of M_z with Re for Ω = 400 rpm, ω = 4000 rpm, θ = 20°, while Figure 2 relates to the spin frequency ω = 4800 rpm. In both Figures we see that the maximum despin moment for the non-Newtonian liquid (solid curves) is attained at very low Reynolds numbers, much lower than for the Newtonian case. Although the peak values are not as great as in Figure 6, the general picture is consistent with that result.

Figure 23 also relates to Liquid 2 and shows the variation of M_z with spin rate for some different values of coning angle and coning rate. The curve labelled 1 relates to the case Ω = 500 rpm, θ = 20°, the curve

labelled 2 relates to the case Ω = 300 rpm, θ = 20°; and the curve labelled 3 relates to the case Ω = 500 rpm, θ = 10°. The following facts are apparent from a study of these Figures: the roll moment decreases with increasing ω with the other quantities held fixed; at fixed ω and fixed θ an increase in coning rate from 300 rpm to 500 rpm results in an increase in M_z; at fixed ω and fixed Ω an increase in θ from 10° to 20° results in an increase in M_z.

For the purposes of detailed analysis, the data shown in Figure 23 is presented for all three components of the moment in Tables 3-5.

9. DISCUSSION

In reviewing the work performed in this project we note several salient features that merit further discussion.

The first issue is the relationship between the results obtained by the approximation technique of Section 5 and the finite element computations of Section 7. In discussing this question we leave aside temporarily whether the fluid is Newtonian or non-Newtonian, since the question arises equally in both cases.

More specifically the point is, how accurate are the results obtained by the methods of Section 5 as presented in Section 6? The procedure used in Section 5 involves two distinct approximations (and consequently two distinct potential sources of error): it is assumed that the cylinder is infinitely long, and it is assumed that the coning rate/spin rate ratio is so small as to allow a perturbation in powers of this ratio, η, with only the leading order terms retained. It should be emphasized that these two assumptions are completely independent, and a solution could formally be obtained with only one of these being invoked. The infinite-length assumption, as shown in Section 4, directly invalidates any calculation of the components M_x and M_y of the moment because of the loss of rigid end-wall conditions, but leaves the possibility of a sufficiently accurate result for the despin moment M_z. The assumption that η is small on the other hand, introduces an error in the determination of the velocities and pressure, and hence of all the moments, but this error tends to zero as $\eta \to 0$.

The finite element computation gives an accurate solution provided only that the physical domain is sufficiently well resolved, that is, that the mesh is fine enough. The mesh used in our calculations was tested extensively and found to be adequate for the range of Reynolds numbers under consideration. Therefore we regard our computational results as highly accurate, especially at lower Reynolds numbers.

As one indication of the validity of the infinite-cylinder, small η perturbation solution, we show in Table 6 values for the despin moment calculated by the two methods. The results refer to a Newtonian liquid, with $b = 4.368$, $\theta = 20°$ and $\eta = 1/6$. The perturbation results are taken from Figure 6, converted using the formula (6.1), while the computational results are those shown in Figure 13. We see from this Table that the values differ by between 5% and 25%, depending on Reynolds number, and that the maximum of the despin moment occurs at about Re = 20 in one case and at about Re = 40 in the other.

The second major issue is that of the appropriate representation of the non-Newtonian behavior of a liquid. There are two aspects to this: selection of a suitable constitutive relation and determination of the parameters to be inserted in this relation. It is crucial, moreover, that the relation and the parameters be appropriate for the type of flow under consideration. In our view, a constitutive relation, with parameters, that has been determined and tested fo[r] [a] different type of flow may well be completely irrelevant for some ot[her] [ty]pe of flow.

This situation poses a major dilemma for the present project. On a general level we are unaware of any constitutive relations that have been

verified (as against postulated) for fully three-dimensional flows of the type under study here. For this reason we were not in a position to hypothesize a constitutive law that could be subject to experimental comparison. On a specific level, for the two liquids of direct interest the information available regarding their non-Newtonian behavior was obtained from simple-shear experiments, and may or may not be relevant to the flow in a spinning and coning cylinder.

As a consequence of this we cannot be certain whether the results obtained in our computations have quantitative validity. On the other hand we feel that they do predict correct behavior qualitatively; this is because there is general qualitative agreement between the computations based on the experimental data and the approximate analysis in Section 5 based on a number of different theoretical models. The most important feature that emerges uniformly is that the maximum despin moment occurs at a significantly lower Reynolds number in a non-Newtonian fluid than in a Newtonian fluid.

In order to obtain computational results that could be quantitatively reliable it would be necessary to determine a constitutive law and parameters valid for the flow in question. This would not be easy to do with any degree of certainty. The analysis of Section 5 can be helpful; it shows that beginning with various different models one arrives for small enough η at a relation that involves a complex viscosity. The latter is a quantity that can be measured from stress relaxation or torsional rheogoniometer experiments. At the same time it must be said that a complex viscosity law, which is a linear law, may be insufficient. The non-

linear law of shear thinning used in the computations led to significant effects, which would not have been the case if the response of the liquid were primarily linear-elastic. This may be attributed to the following fact. A typical dilute polymer solution has a relaxation time of about 0.05 - 0.1 sec. For a large spin rate of 4000-6000 rpm, the Weissenberg number as defined by equation (2.6) will lie in the range 20-60, which is very large in terms of standard viscoelastic models. In fact, the perturbation procedure of Section 5 breaks down at such large Weissenberg numbers. These observations suggest an appropriate empirical law should incorporate both the elastic effects giving rise to complex viscosity and nonlinear effects due to the large Weissenberg number.

In summary therefore, we believe that the finite element method as implemented in the code FIDAP provides accurate solutions to the problem of non-Newtonian fluid flow in a coning and spinning cylinder; reliable quantitative results await the empirical determination of a suitable constitutive law.

REFERENCES

W.O. Criminale, J.L. Ericksen and G.L. Filbey, *Arch. Rat. Mech. Anal.*, 1, 410, 1958.

W.P. D'Amico Jr. and M.C. Miller, *J. Spacecraft & Rockets*, 16, 62, 1979.

T. Herbert, CRDC Final Report, Contract DAAK11-83-K-0011, July 1985.

M.C. Miller, *J. Guidance, Control & Dynamics*, 5, 151, 1982.

J.G. Oldroyd, *Proc. Roy. Soc. A*, 245, 278, 1958.

K. Stewartson, *J. Fluid Mechanics*, 5, 577, 1959.

H.R. Vaughn, W.L. Oberkampf and W.P. Wolfe, *J. Fluid Mechanics*, 150, 121, 1985.

E.H. Wedemeyer, B.R.L. Report No. 1325, 1966.

Re	M_x	$\bar{M}_y$	M_z	M_z/M_x
10	.05953	.02807	.02202	.3699
20	.07791	.06560	.02860	.3671
30	.08056	.09023	.02946	.3657
40	.07982	.10545	.02918	.3656
60	.07654	.12556	.02805	.3665
80	.07303	.13854	.02681	.3671
100	.06975	.14793	.02562	.3673
120	.06669	.15532	.02450	.3674
150	.06288	.16327	.02311	.3675
175	.05984	.16885	.02200	.3676
200	.05729	.17310	.02108	.3680
300	.04921	.18448	.01817	.3692
400	.04361	.19069	.01619	.3712
500	.03945	.19437	.01472	.3731
750	.03244	.19805	.01229	.3789
1000	.02804	.19768	.01080	.3852

Table 1: Moments for a Newtonian liquid in a cylinder of aspect ratio 4.368, coning angle 20°, coning/spin ratio 1/6

Liquid 1		Liquid 2	
Shear rate (sec^{-1})	Viscosity (poise)	Shear rate (sec^{-1})	Viscosity (poise)
.855	8.011	.017	1307.349
1.707	7.937	.034	1216.849
3.407	7.488	.067	1125.913
6.798	7.271	.135	1022.781
13.564	6.818	.27	942.722
27.064	5.892	.54	797.31
54.	4.872	1.077	651.202
107.744	4.07	2.149	504.397
214.977	3.152	4.289	371.76
428.937	2.49	8.558	257.124
679.819	2.087	17.076	161.551

Table 2: Experimental data for variation of viscosity with shear rate for two liquids

ω rpm	η	Re	M_x	$\bar{M}_y$	M_z
1000	.5	1.7	.66036	.368902	.24118
2000	.25	3.4	.18870	.195367	.068612
3000	.1667	5.1	.081789	.111845	.029732
4000	.125	6.8	.043971	.071511	.016001
5000	.1	8.5	.027316	.049646	.009950
6000	.0833	10.2	.017866	.0362349	.0065039
7000	.07143	11.9	.012591	.027650	.004585
8000	.0625	13.6	.0092860	.0217832	.0033782
9000	.05556	15.3	.0070814	.0175939	.0025752
10000	.05	17.0	.005546	.014488	.002016

Table 3: LIQUID 2 - Coning rate Ω = 500 rpm, Coning angle θ = 20°

ω rpm	η	Re	M_x	$\tilde{M}_y$	M_z
1000	.3	1.7	.23166	.113717	.083304
2000	.15	3.4	.067447	.071241	.024475
3000	.1	5.1	.028997	.040781	.010542
4000	.075	6.8	.015686	.026023	.005706
5000	.06	8.5	.009542	.017878	.003479
6000	.05	10.2	.0064163	.0131311	.0023306
7000	.04286	11.9	.004534	.0099828	.0016464
8000	.0375	13.6	.0033457	.0078472	.0012149
9000	.033[illegible]	15.3	.0025481	.00631841	.00092651
10000	.03	17.0	.002003	.005196	.000728

Table 4: LIQUID 2 - Coning rate Ω = 300 rpm, Coning angle θ = 20°

ω rpm	η	Re	M_x	$\tilde{M}_y$	M_z
1000	.5	1.7	.34027	.160873	.059135
2000	.25	3.4	.10254	.103172	.017882
3000	.1667	5.1	.043883	.0600640	.0077028
4000	.125	6.8	.023523	.0383475	.0041432
5000	.1	8.5	.014343	.0266239	.0025288
6000	.0833	10.2	.0095728	.0195625	.0016808
7000	.07143	11.9	.0067004	.0149356	.0011818
8000	.0625	13.6	.0049337	.0117658	.000869
9000	.05556	15.3	.0037631	.009499	.000663
10000	.05	17.0	.0029458	.007813	.000519

Table 5: LIQUID 2 - Coning rate Ω = 500 rpm, Coning angle θ = 10°

Re	M_z finite cylinder computation	M_z infinite cylinder approximate solution
10	.02202	.02656
20	.02860	.03043
30	.02946	.02882
40	.02918	.02690
60	.02805	.02386
80	.02681	.02268
100	.02562	.01998
120	.02450	.01865
150	.02311	.01709
200	.02108	.01520

Table 6: Comparison of despin moments obtained from finite element computation and infinite-cylinder approximate solution

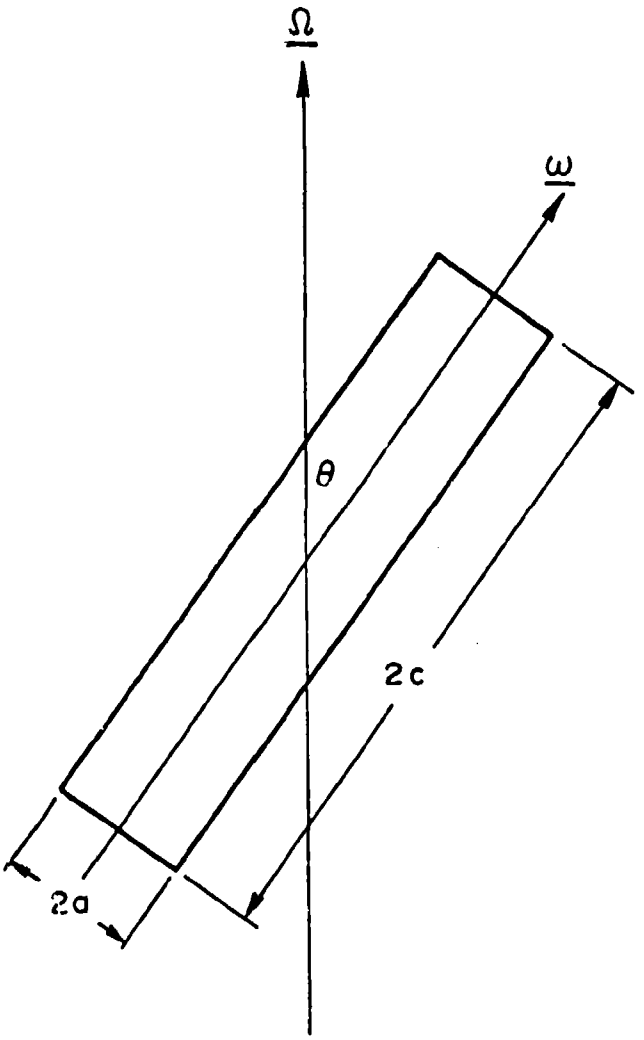

Figure 1: Schematic diagram of the cylinder

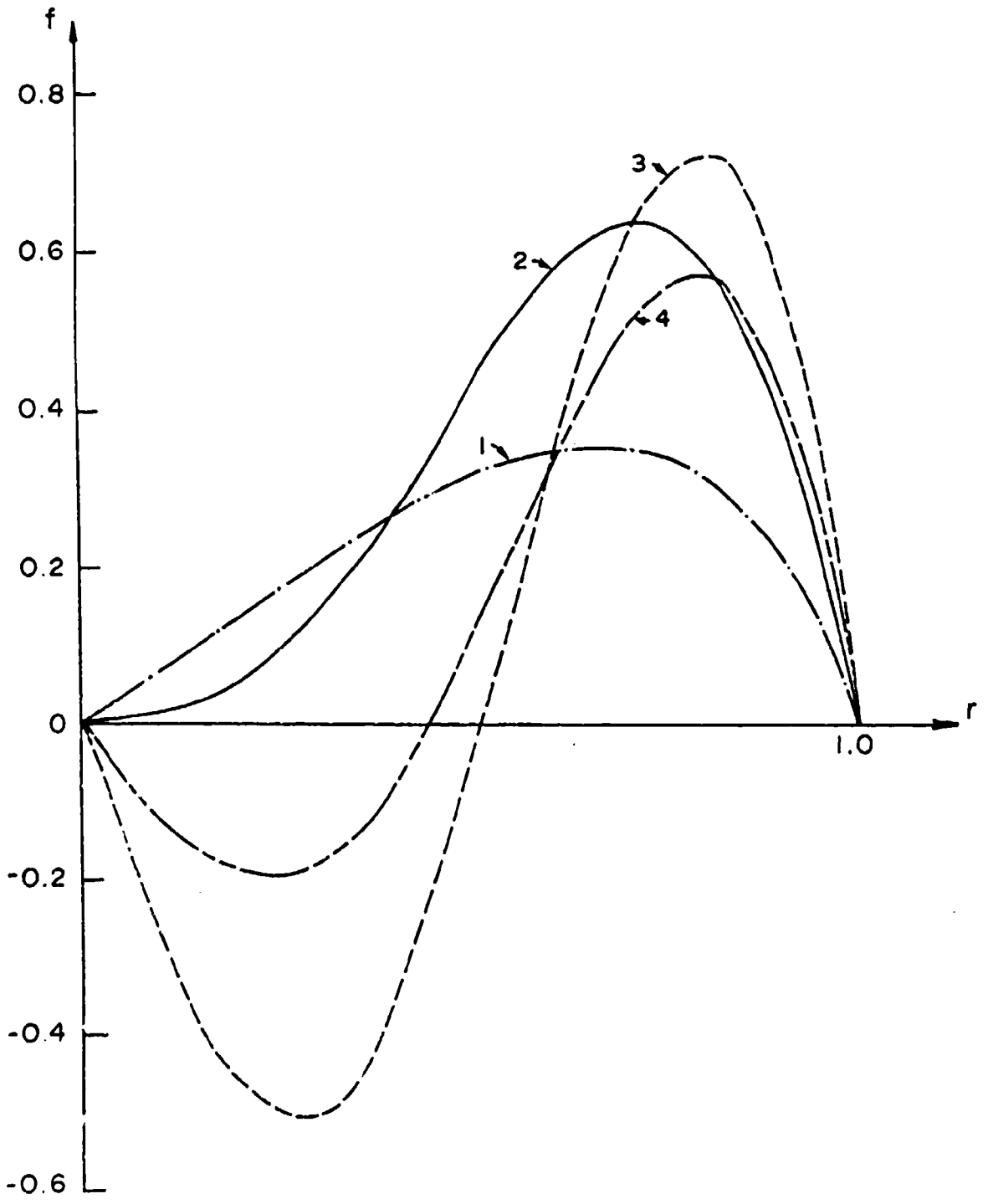

Figure 2: Variation of velocity function f with radius r for viscoelastic fluid, Re = 15

1. Newtonian
2. De = 0.1, ϵ = 0.1
3. De = 0.2, ϵ = 0.1
4. De = 0.2, ϵ = 0.2

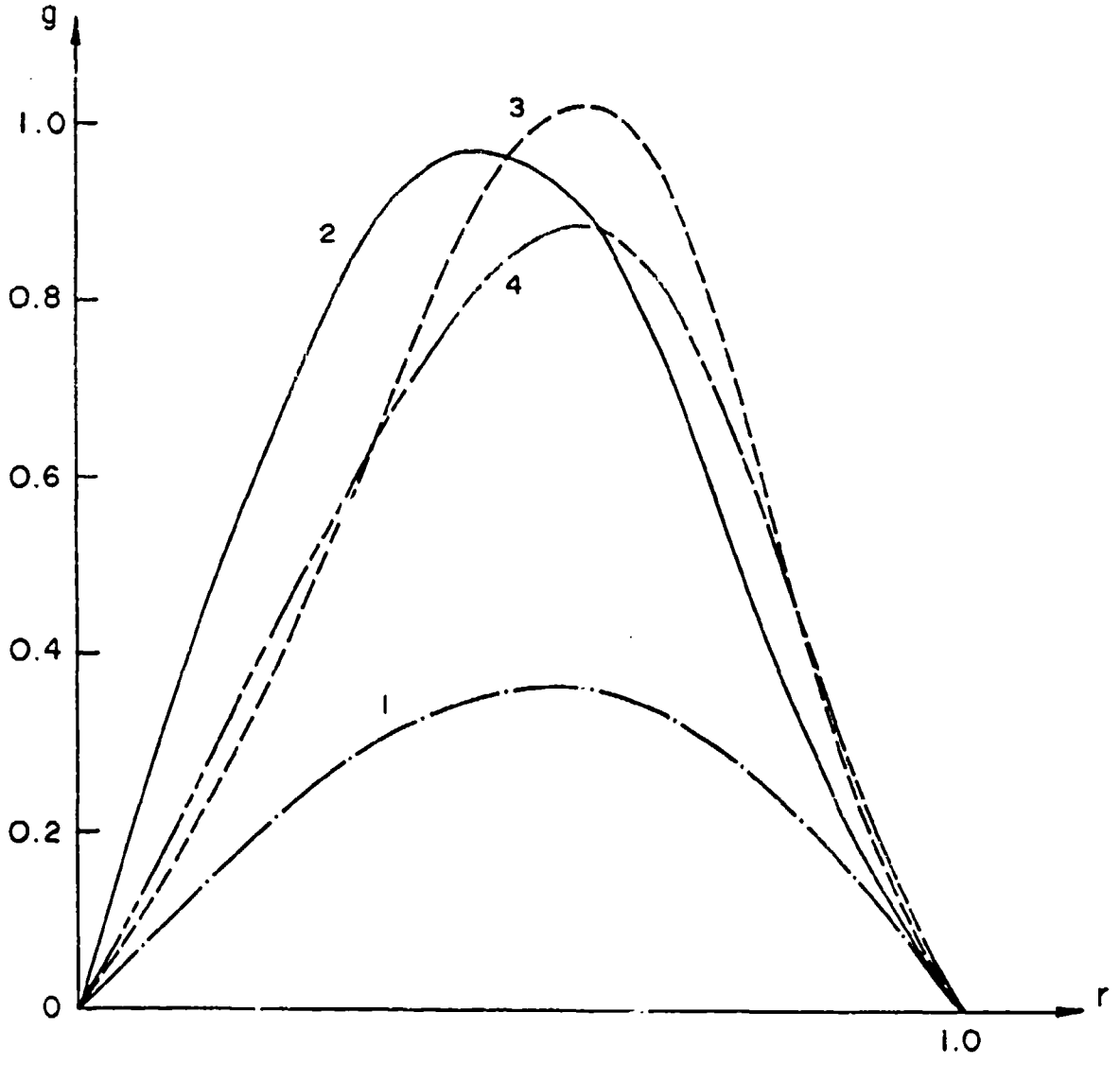

Figure 3: Variation of velocity function g with radius r for viscoelastic fluid, Re = 15

1. Newtonian
2. De = 0.1, ϵ = 0.1
3. De = 0.2, ϵ = 0.1
4. De = 0.2, ϵ = 0.2

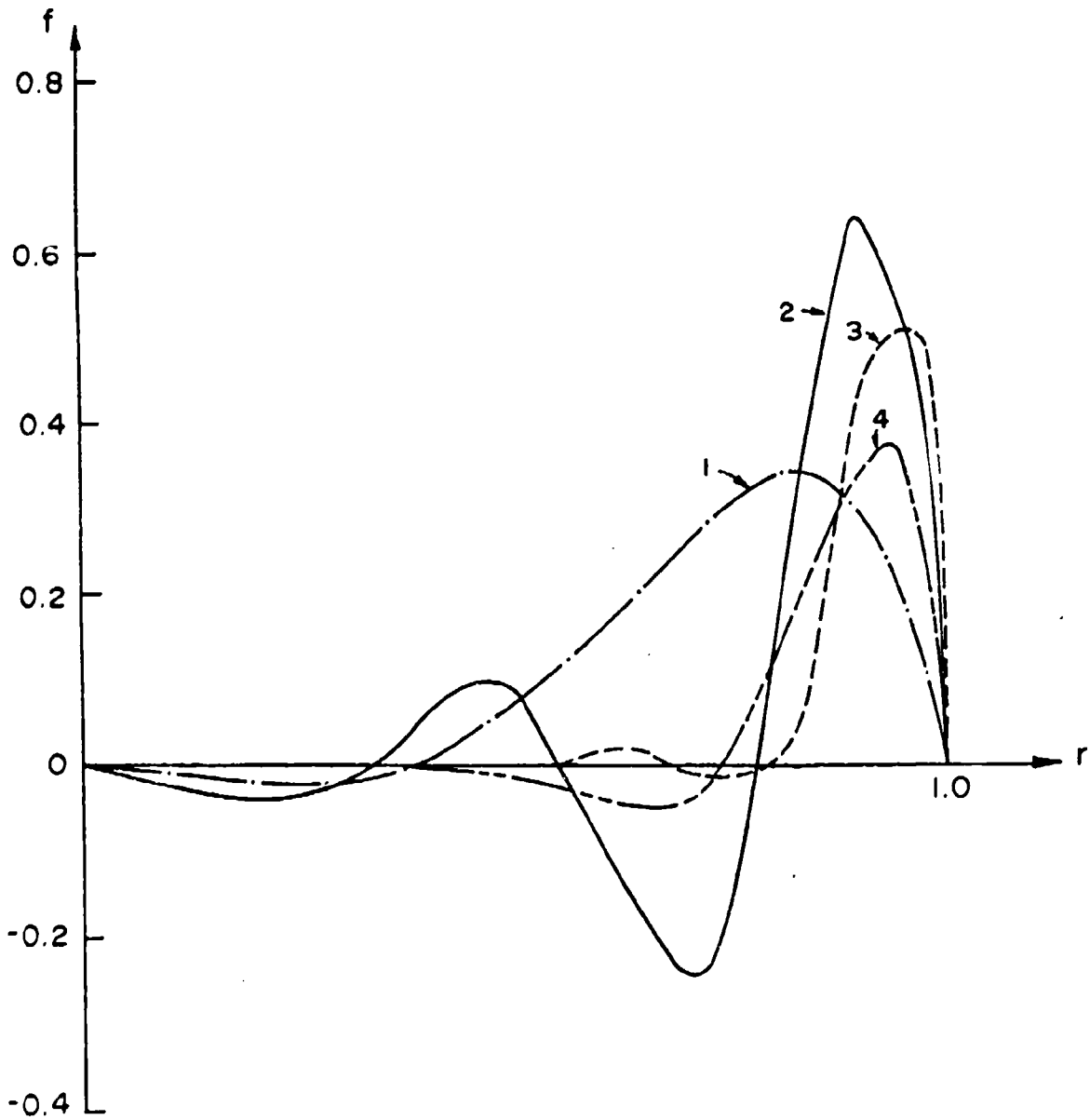

Figure 4: Variation of velocity function f with radius r for viscoelastic fluid, Re = 50

1. Newtonian
2. De = 0.1, ϵ = 0.1
3. De = 0.2, ϵ = 0.1
4. De = 0.2, ϵ = 0.2

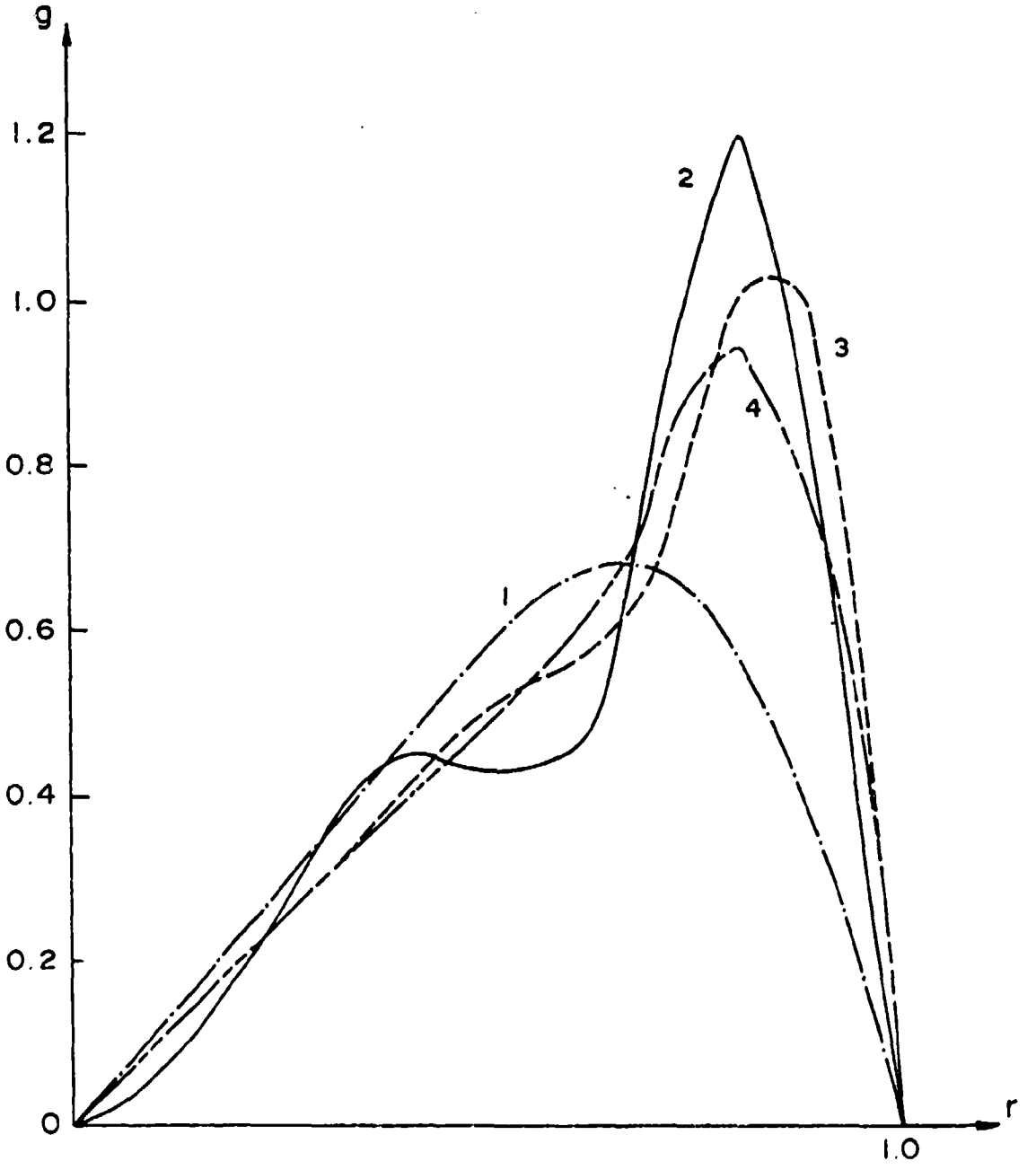

Figure 5: Variation of velocity function g with radius r for viscoelastic fluid, Re = 50

1. Newtonian
2. De = 0.1, ϵ = 0.1
3. De = 0.2, ϵ = 0.1
4. De = 0.2, ϵ = 0.2

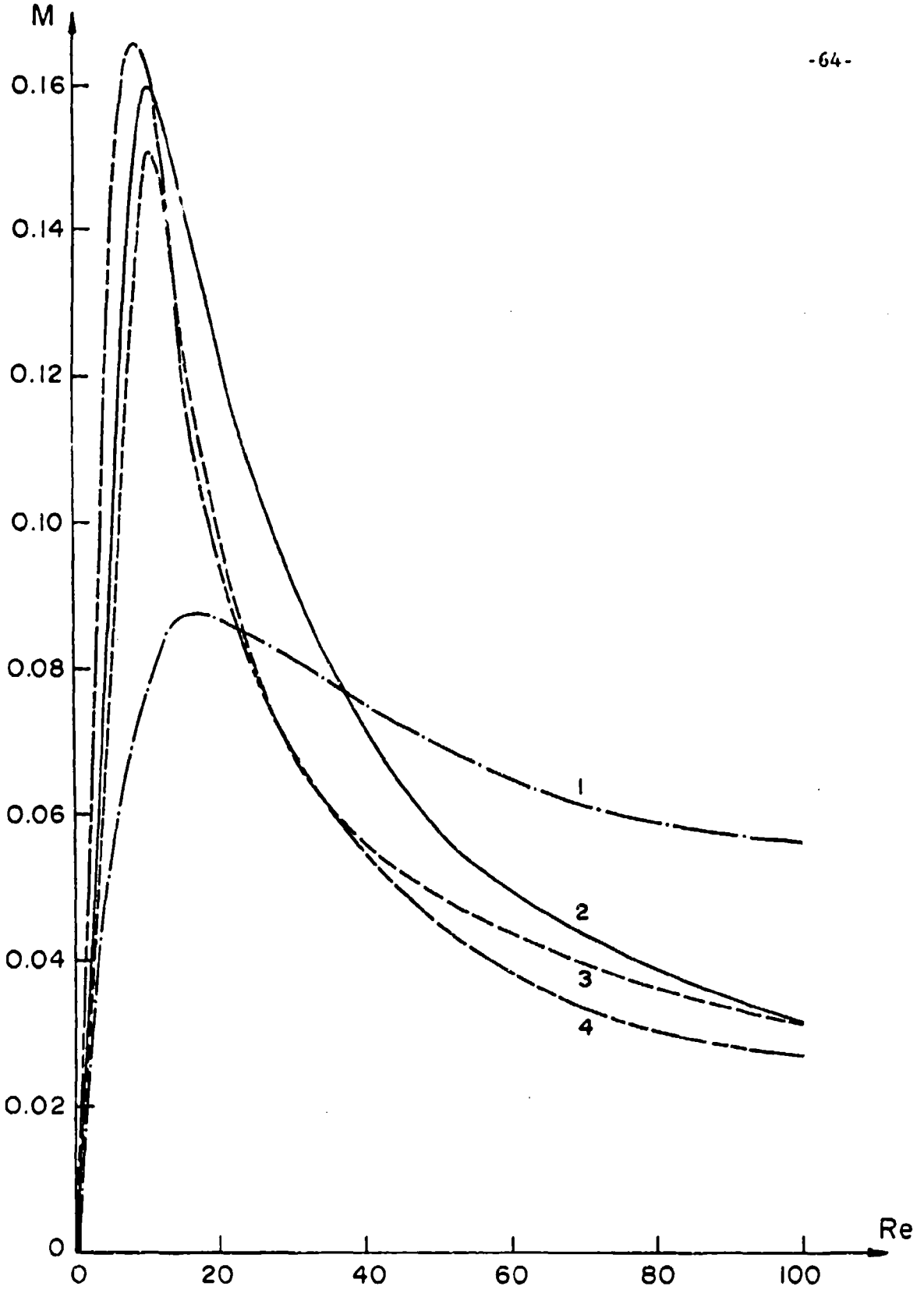

Figure 6: Variation of moment M (equation (6.1)) with Re for viscoelastic fluid

1. Newtonian
2. De = 0.1, ϵ = 0.1
3. De = 0.2, ϵ = 0.1
4. De = 0.2, ϵ = 0.2

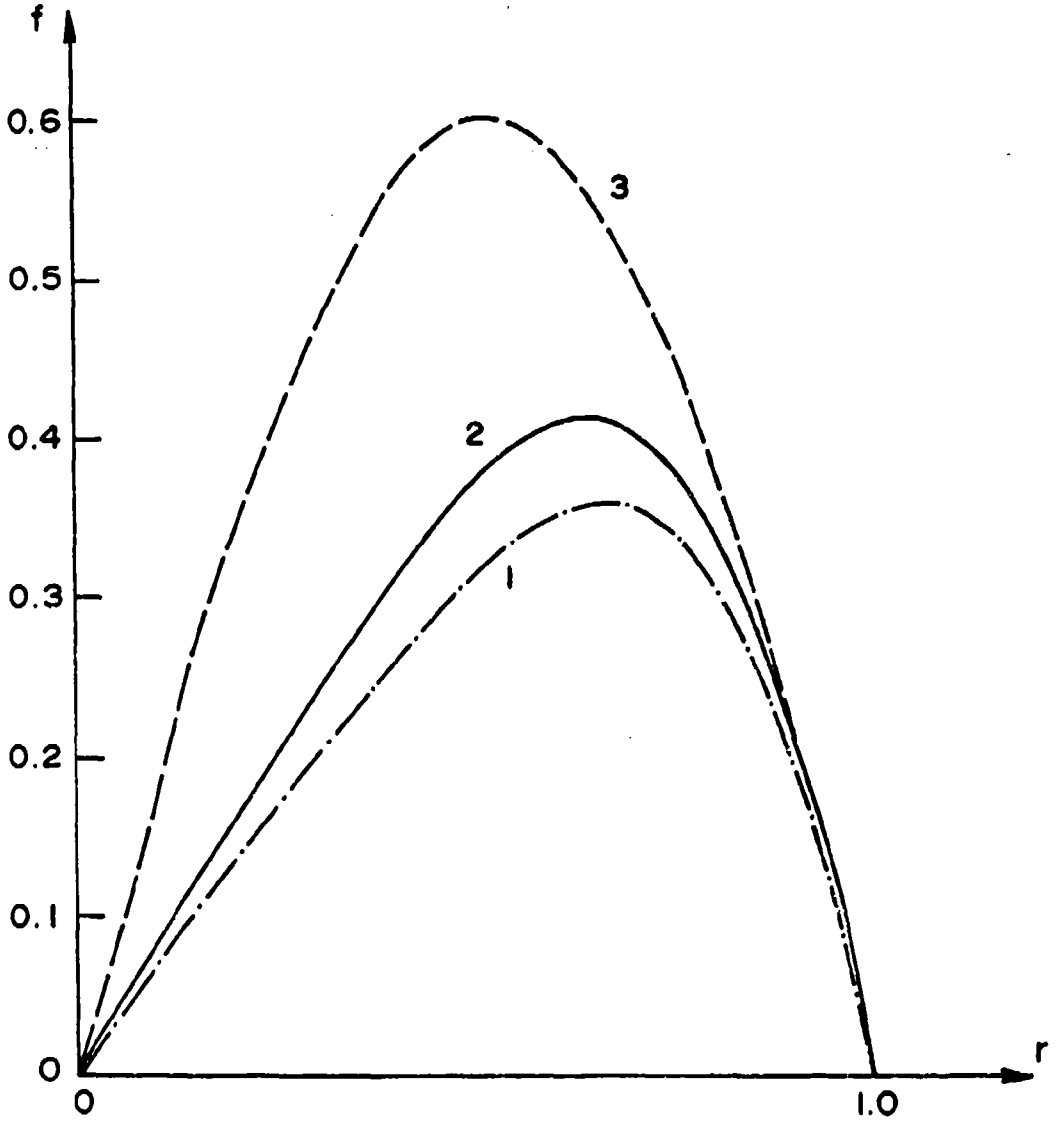

Figure 7: Variation of velocity function f with radius r for second-order fluid, Re = 15

1. Newtonian
2. De = .01
3. De = .1

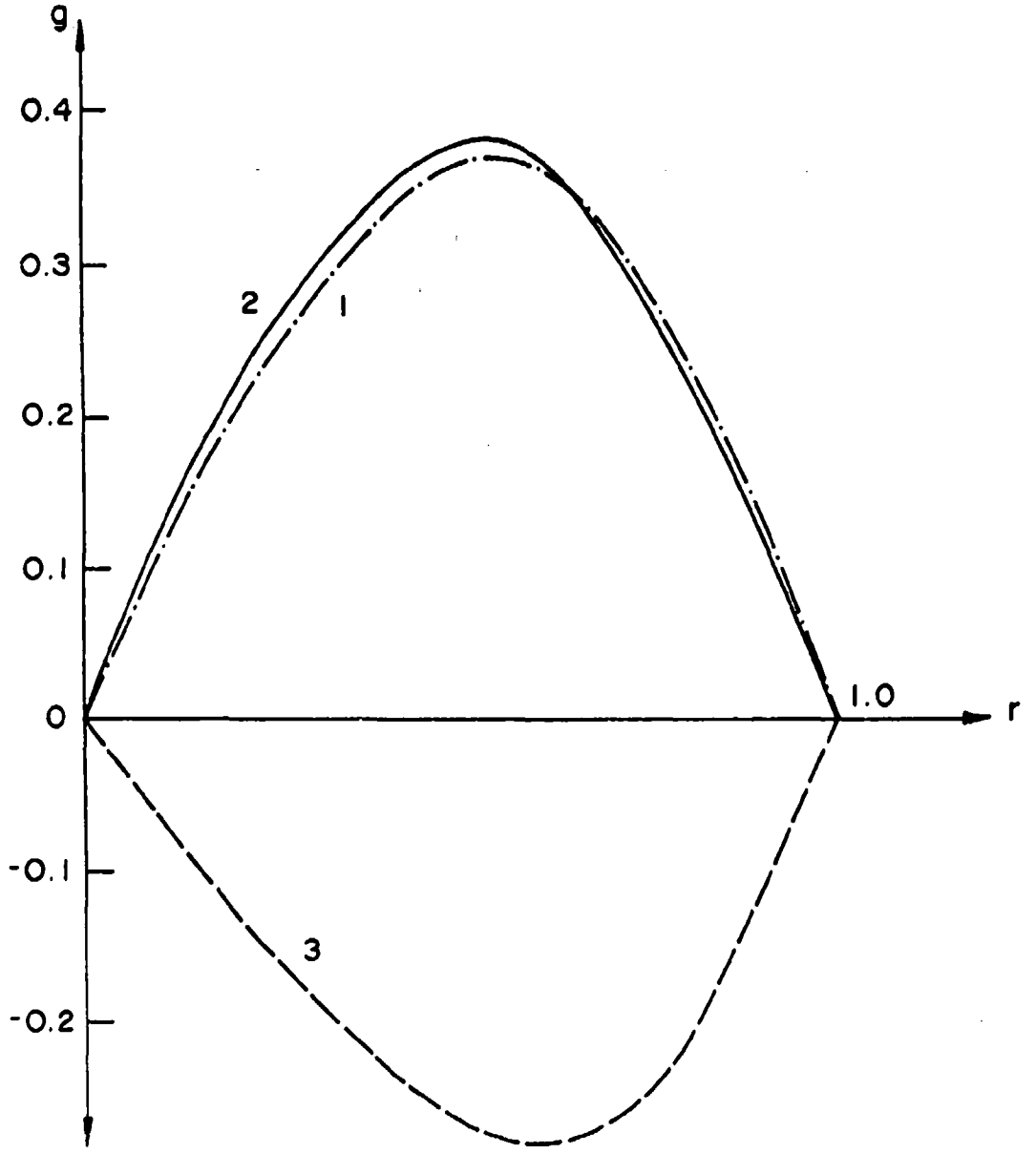

Figure 8: Variation of velocity function g with radius r for second-order fluid, Re = 15

1. Newtonian
2. De = .01
3. De = .1

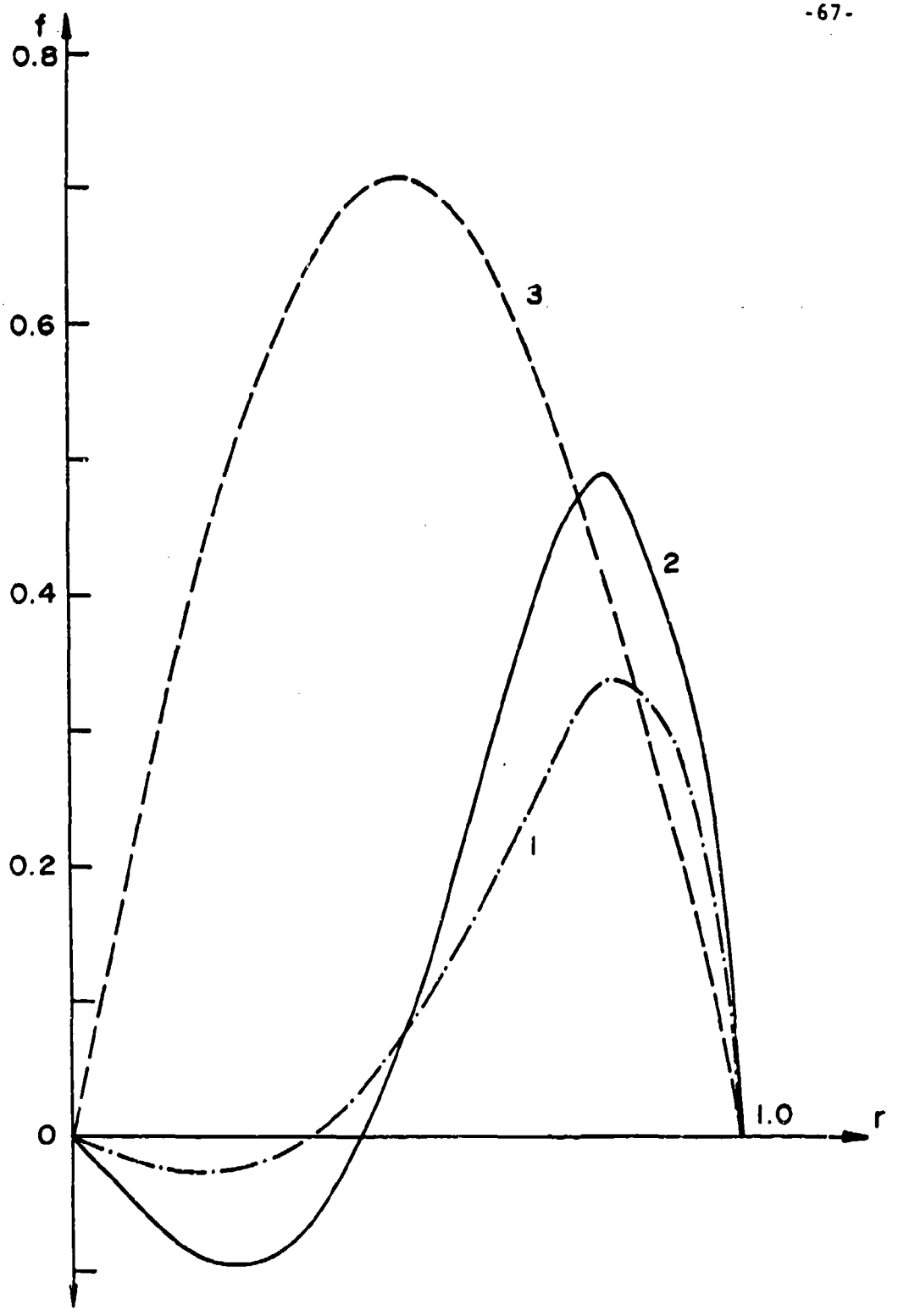

Figure 9: Variation of velocity function f with radius r for second-order fluid, Re = 50

1. Newtonian
2. De = .01
3. De = .1

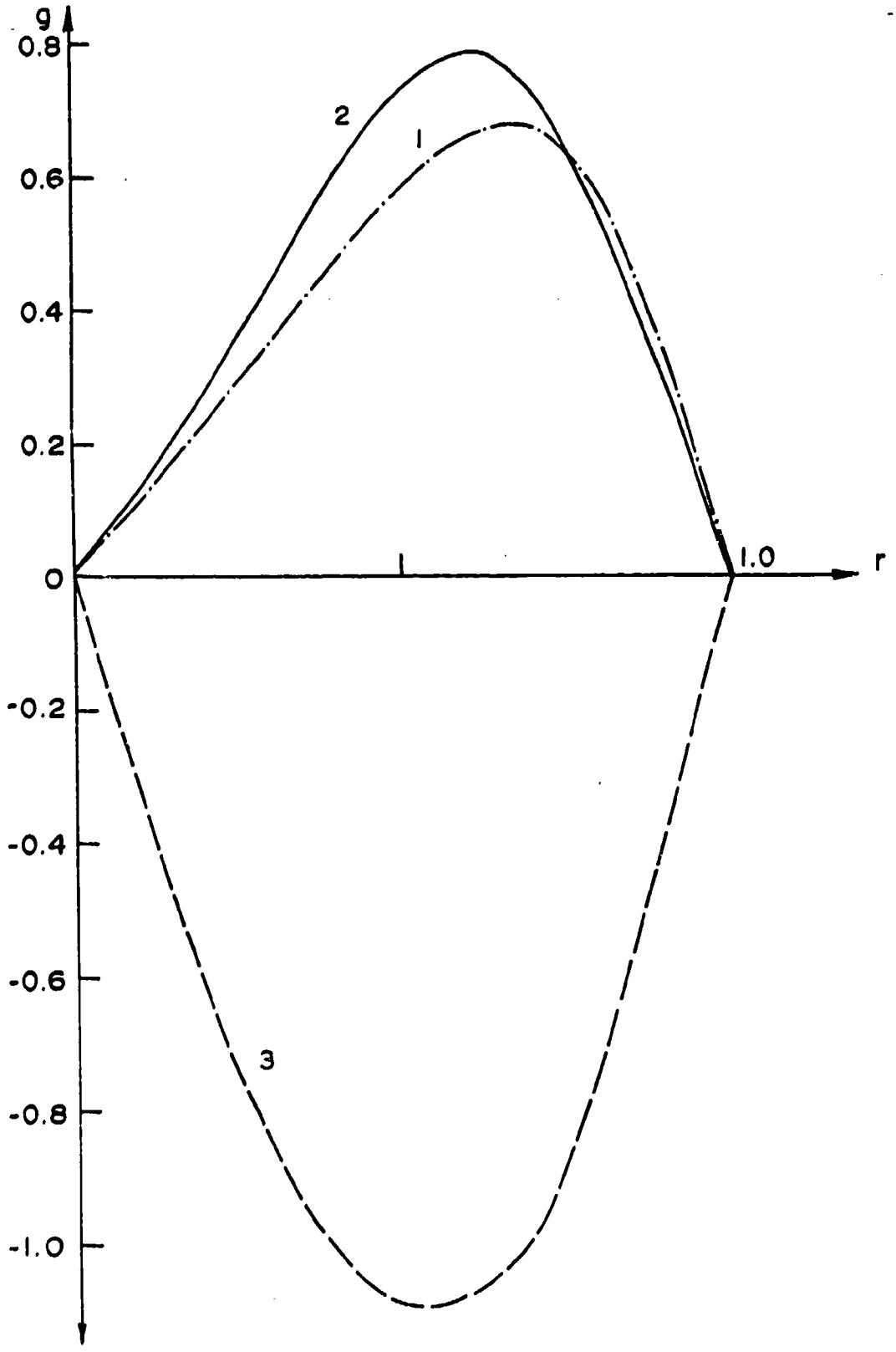

Figure 10: Variation of velocity function g with radius r for second-order fluid, Re = 50

1. Newtonian
2. De = .01
3. De = .1

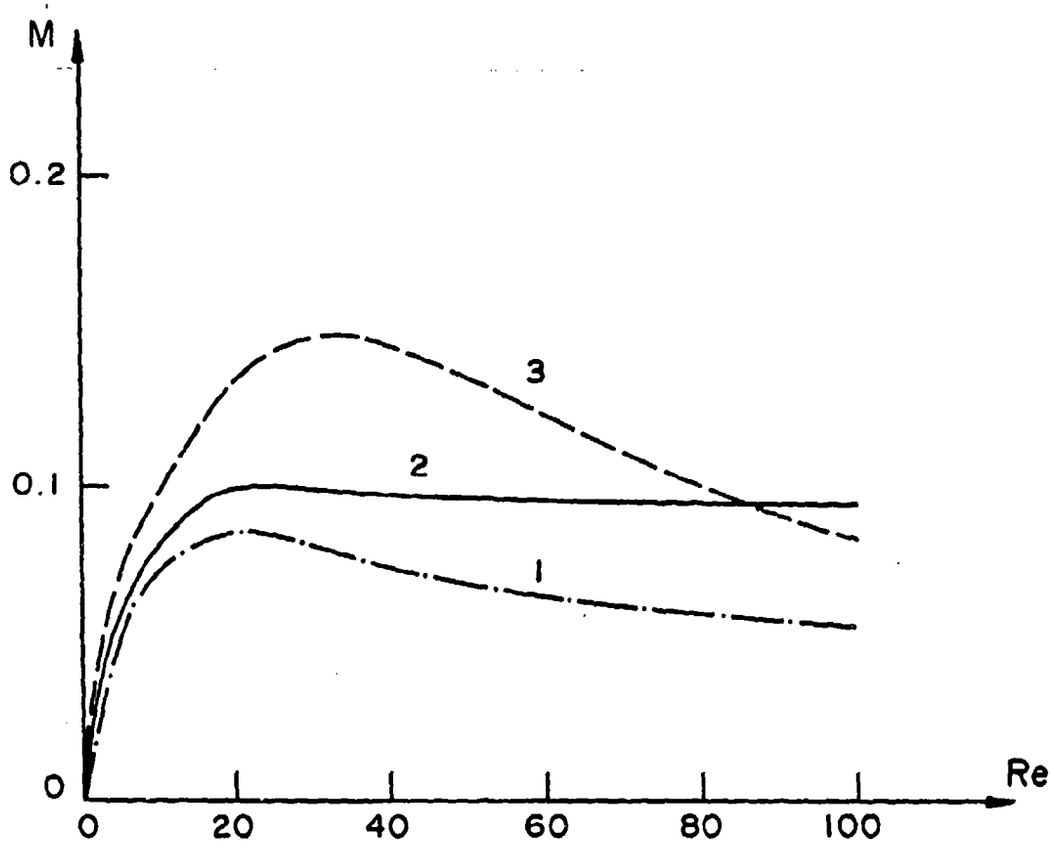

Figure 11: Variation of moment M (equation (6.1)) with Re for second-order fluid

1. Newtonian
2. De = 0.01
3. De = 0.1

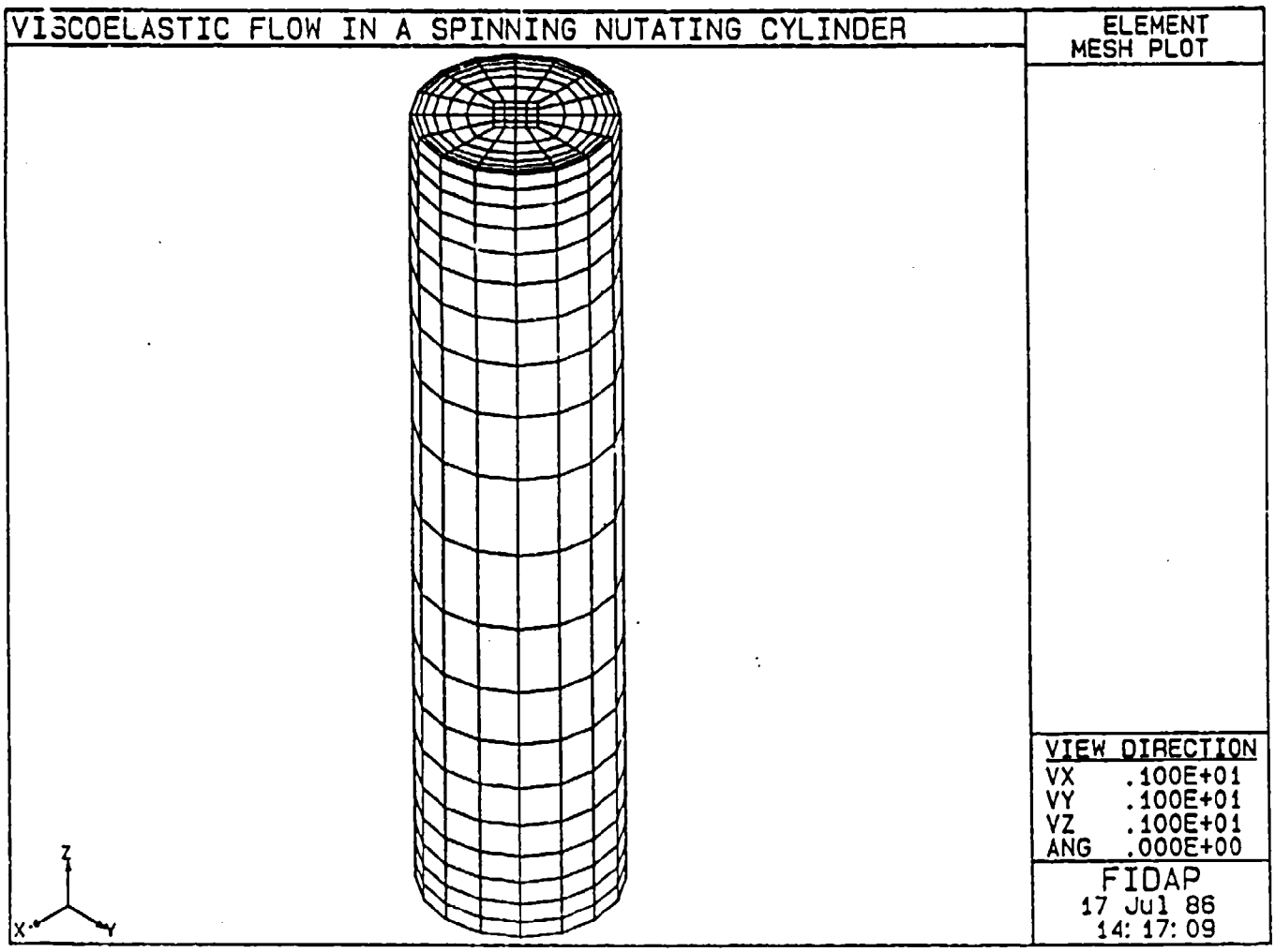
VISCOELASTIC FLOW IN A SPINNING NUTATING CYLINDER
ELEMENT
MESH PLOT
VIEW DIRECTION
VX .100E+01
VY .100E+01
VZ .100E+01
ANG .000E+00
FIDAP
17 Jul 86
14:17:09
Z
X
Y

Figure 12

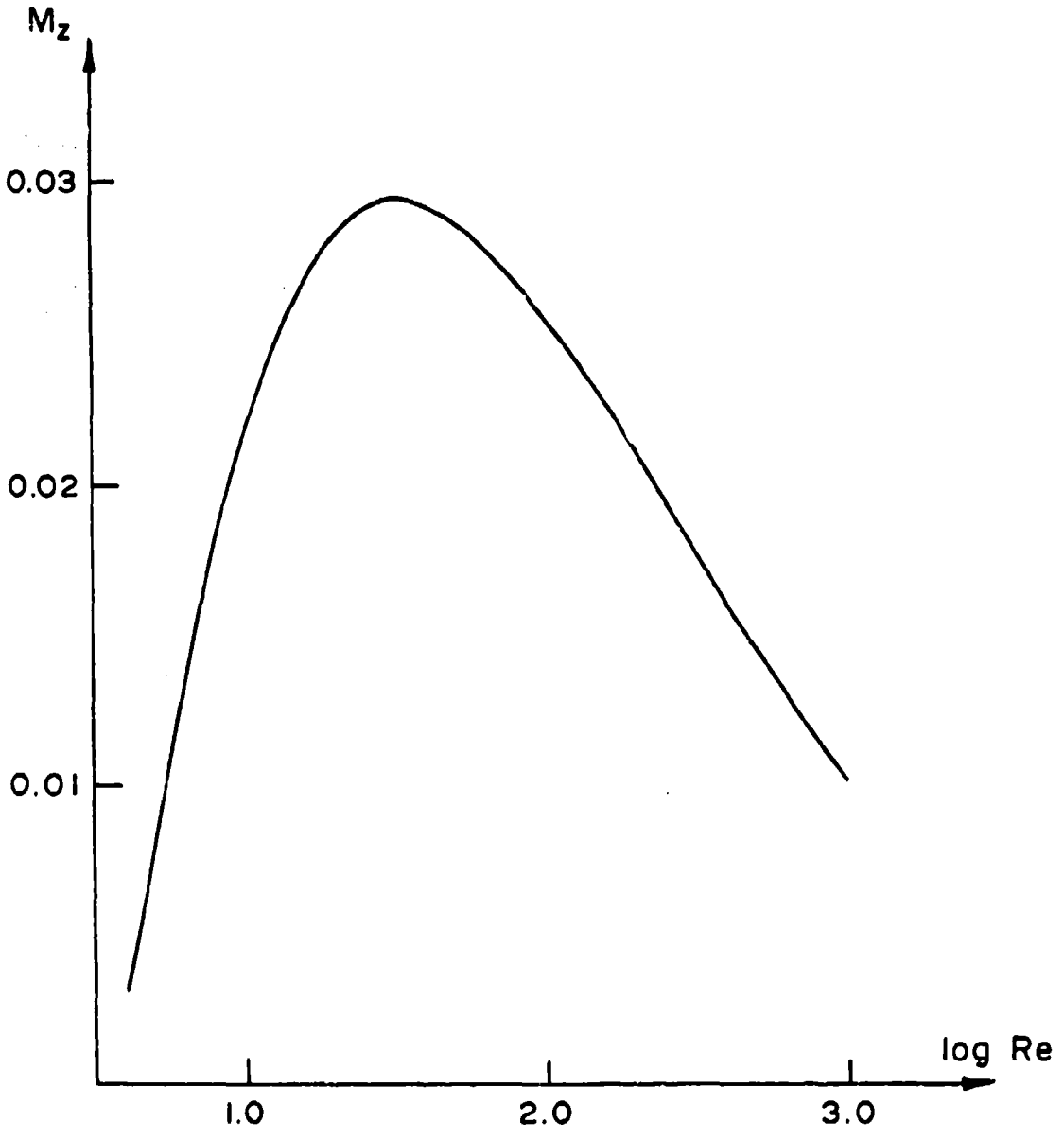

Figure 13: Variation of M_z with Reynolds number for a Newtonian liquid, with $\theta = 20°$, $\eta = 1/6$, $b = 4.368$

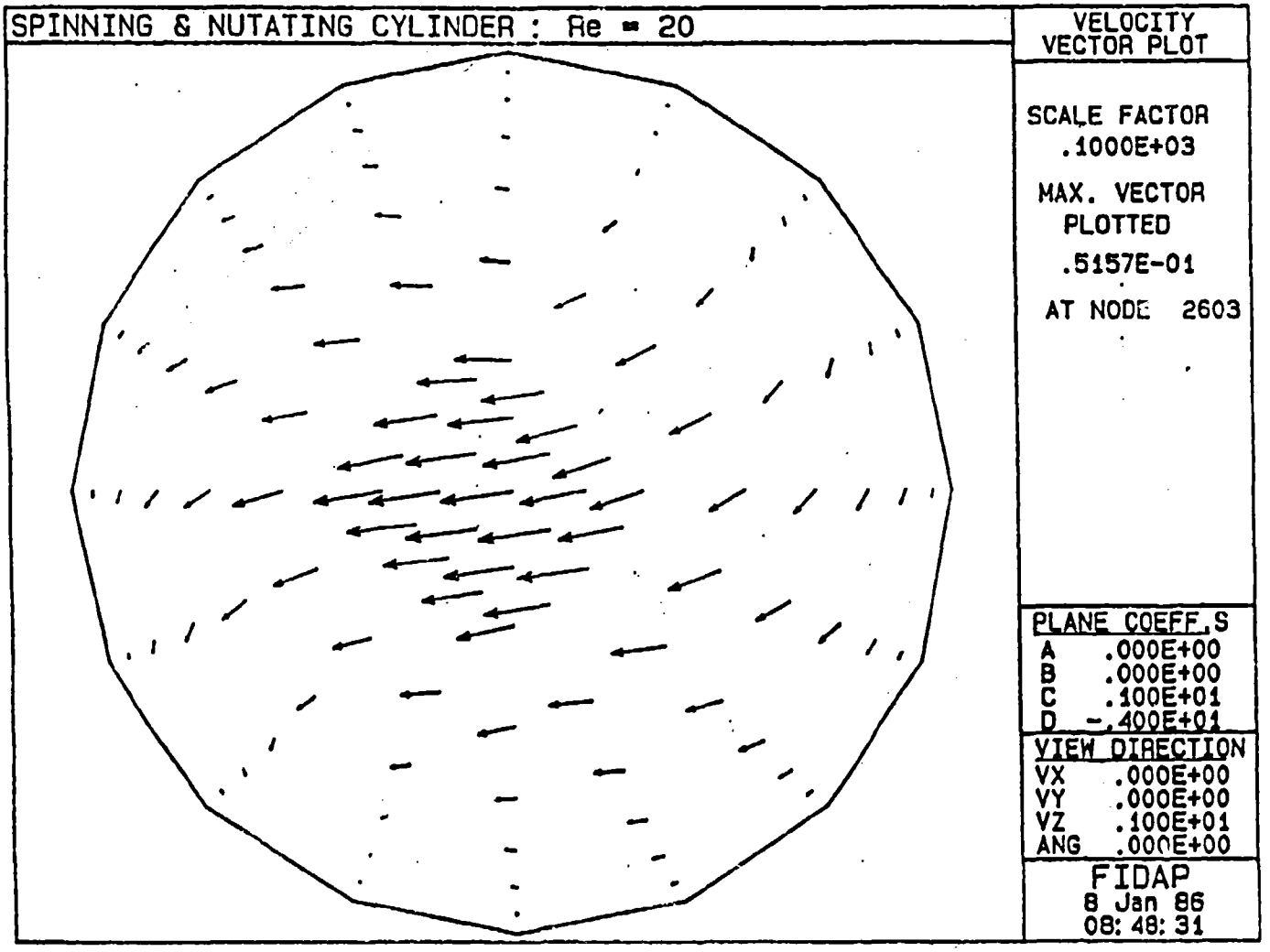
SPINNING & NUTATING CYLINDER : Re = 20
VELOCITY VECTOR PLOT
SCALE FACTOR
.1000E+03
MAX. VECTOR PLOTTED
.5157E-01
AT NODE 2603
PLANE COEFF.S
A .000E+00
B .000E+00
C .100E+01
D -.400E+01
VIEW DIRECTION
VX .000E+00
VY .000E+00
VZ .100E+01
ANG .000E+00
FIDAP
8 Jan 86
08:48:31

Figure 14a

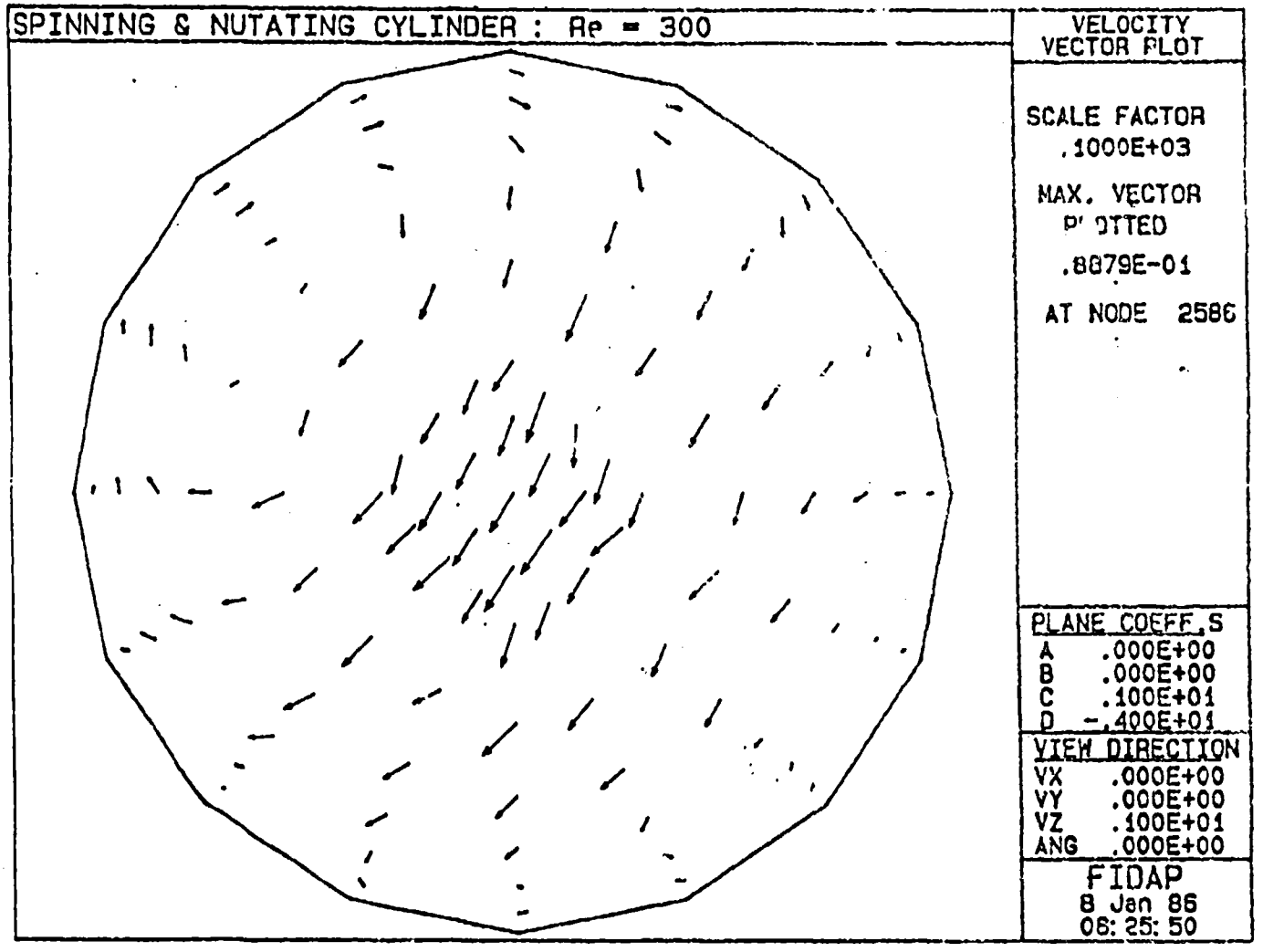
SPINNING & NUTATING CYLINDER : Re = 300
VELOCITY VECTOR PLOT
SCALE FACTOR
.1000E+03
MAX. VECTOR PLOTTED
.8879E-01
AT NODE 2586
PLANE COEFF.S
A .000E+00
B .000E+00
C .100E+01
D -.400E+01
VIEW DIRECTION
VX .000E+00
VY .000E+00
VZ .100E+01
ANG .000E+00
FIDAP
8 Jan 86
06:25:50

Figure 14b

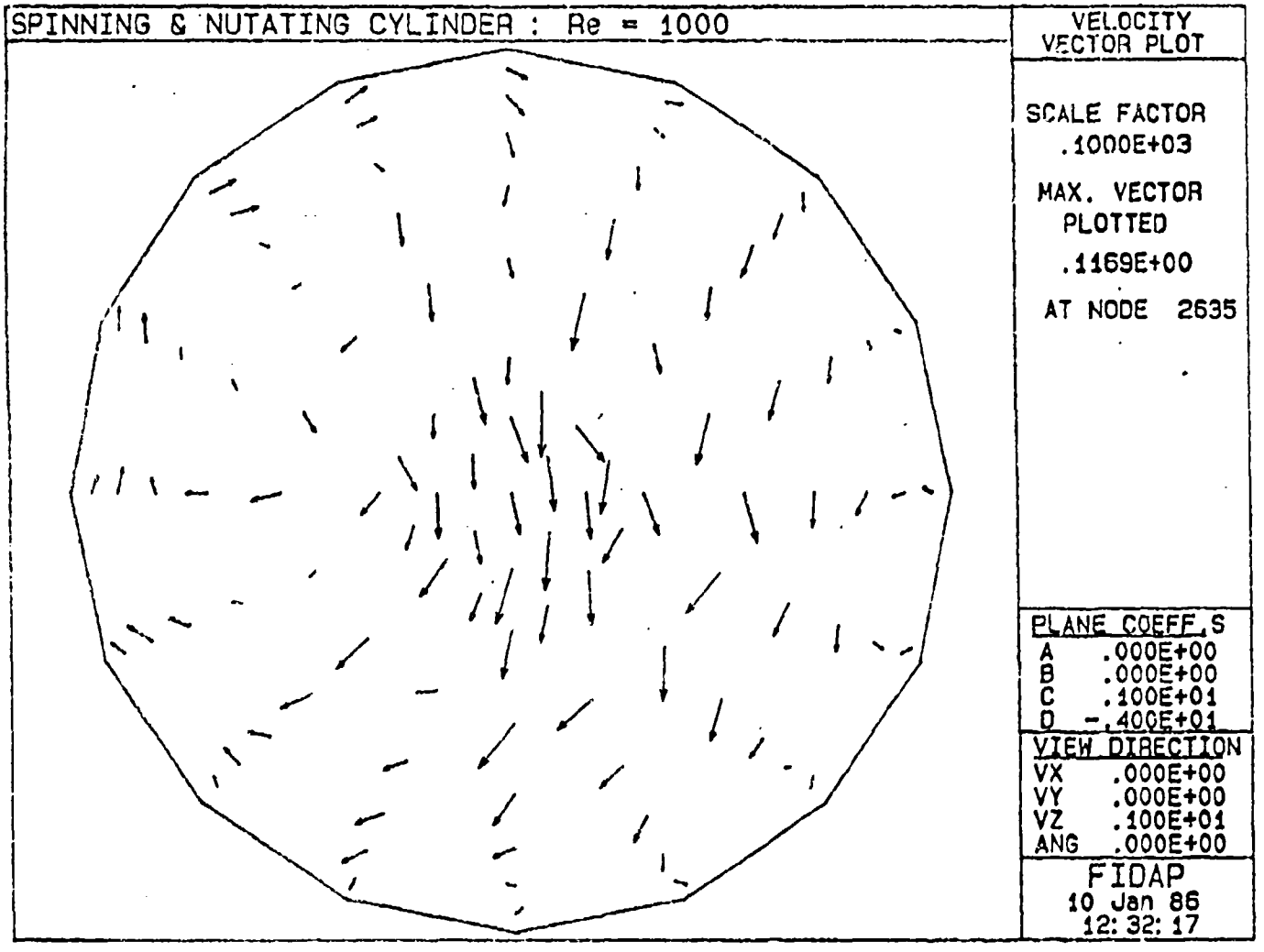
SPINNING & NUTATING CYLINDER : Re = 1000
VELOCITY VECTOR PLOT
SCALE FACTOR .1000E+03
MAX. VECTOR PLOTTED .1169E+00
AT NODE 2635
PLANE COEFF.S
A .000E+00
B .000E+00
C .100E+01
D -.400E+01
VIEW DIRECTION
VX .000E+00
VY .000E+00
VZ .100E+01
ANG .000E+00
FIDAP
10 Jan 86
12:32:17

Figure 14c

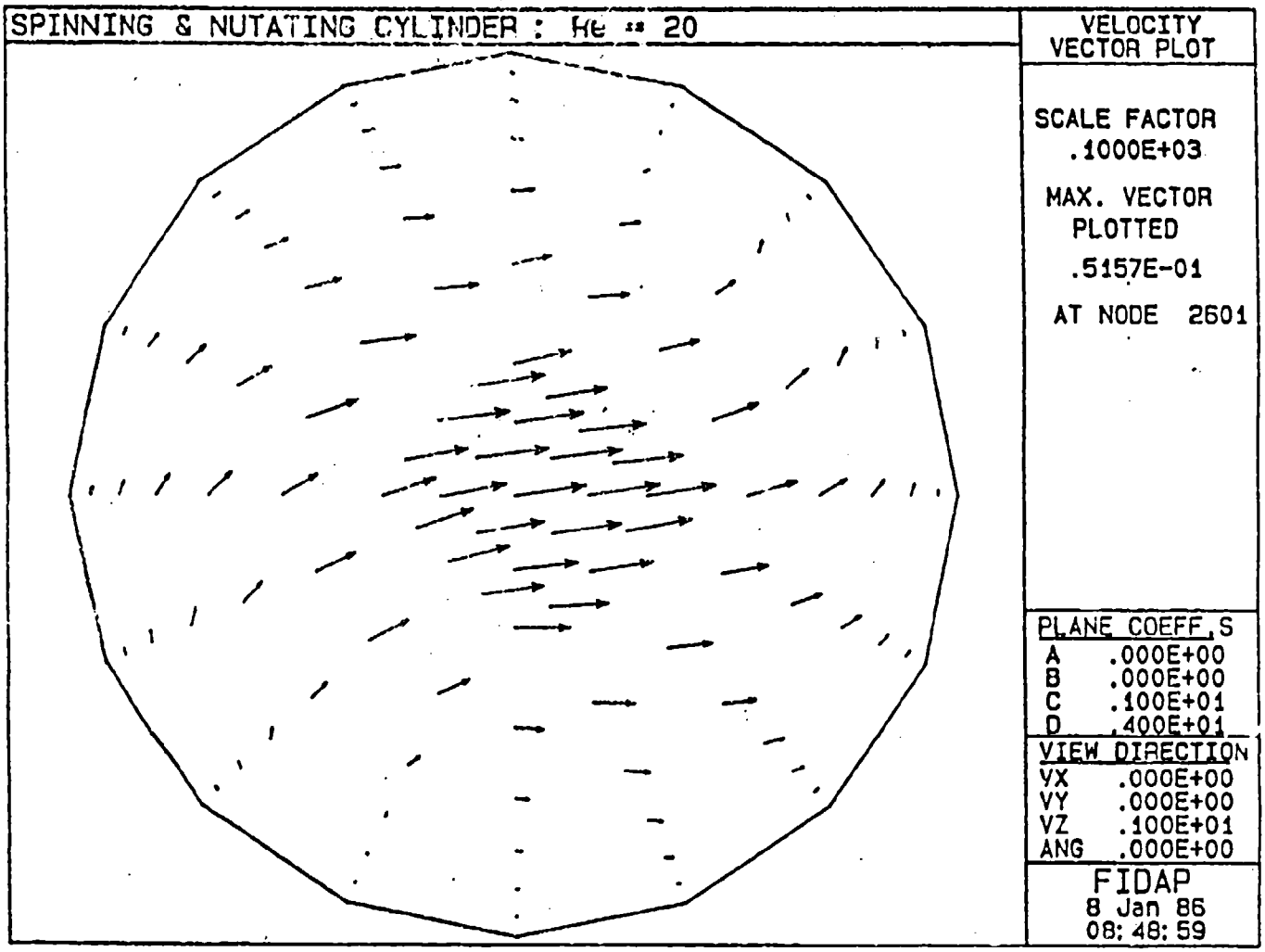
SPINNING & NUTATING CYLINDER : Re = 20
VELOCITY VECTOR PLOT
SCALE FACTOR
.1000E+03
MAX. VECTOR PLOTTED
.5157E-01
AT NODE 2601
PLANE COEFF,S
A .000E+00
B .000E+00
C .100E+01
D .400E+01
VIEW DIRECTION
VX .000E+00
VY .000E+00
VZ .100E+01
ANG .000E+00
FIDAP
8 Jan 86
08:48:59

Figure 15a

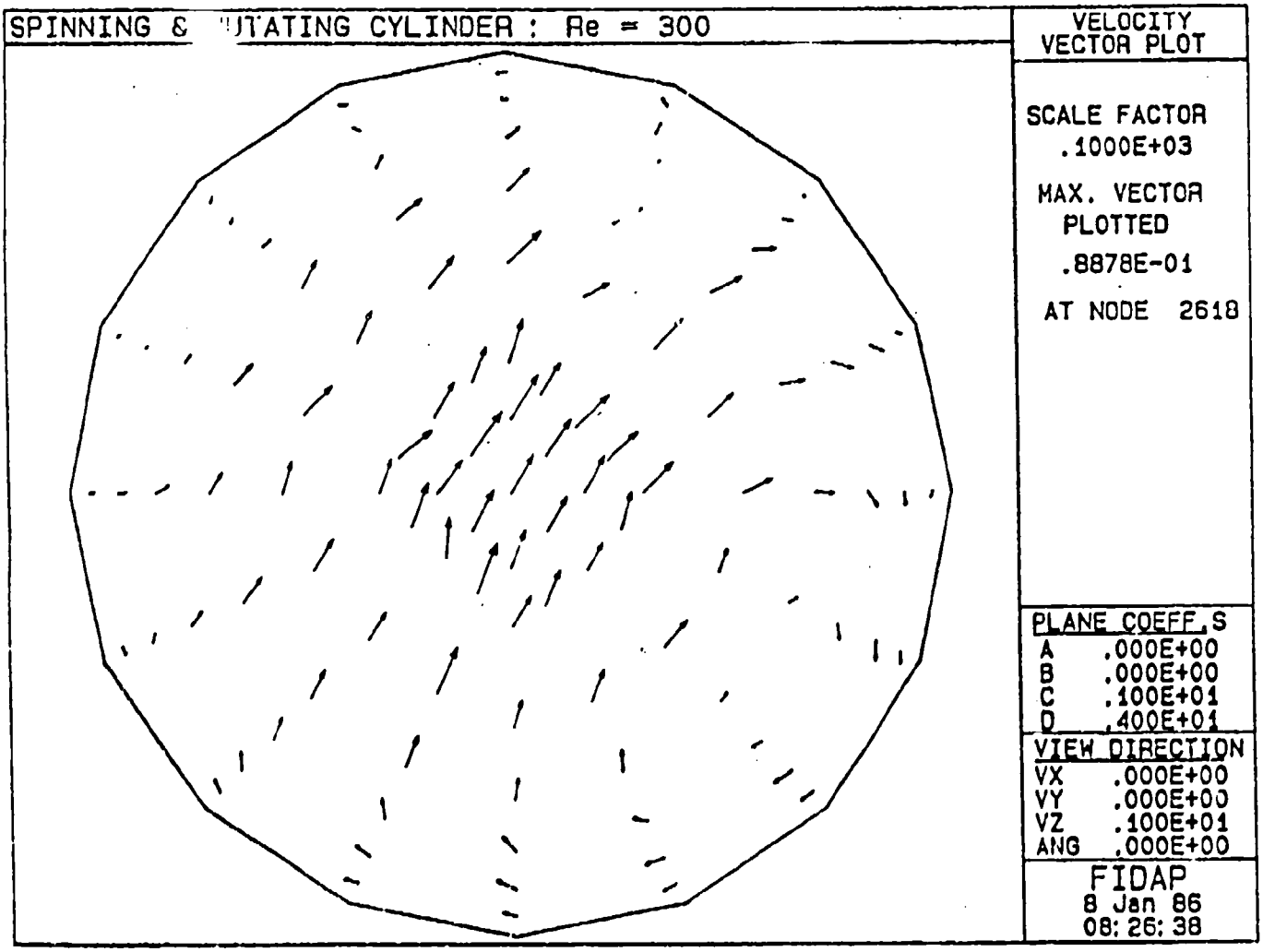
SPINNING & UTATING CYLINDER : Re = 300
VELOCITY VECTOR PLOT
SCALE FACTOR
.1000E+03
MAX. VECTOR PLOTTED
.8878E-01
AT NODE 2618
PLANE COEFF.S
A .000E+00
B .000E+00
C .100E+01
D .400E+01
VIEW DIRECTION
VX .000E+00
VY .000E+00
VZ .100E+01
ANG .000E+00
FIDAP
8 Jan 86
08:26:38

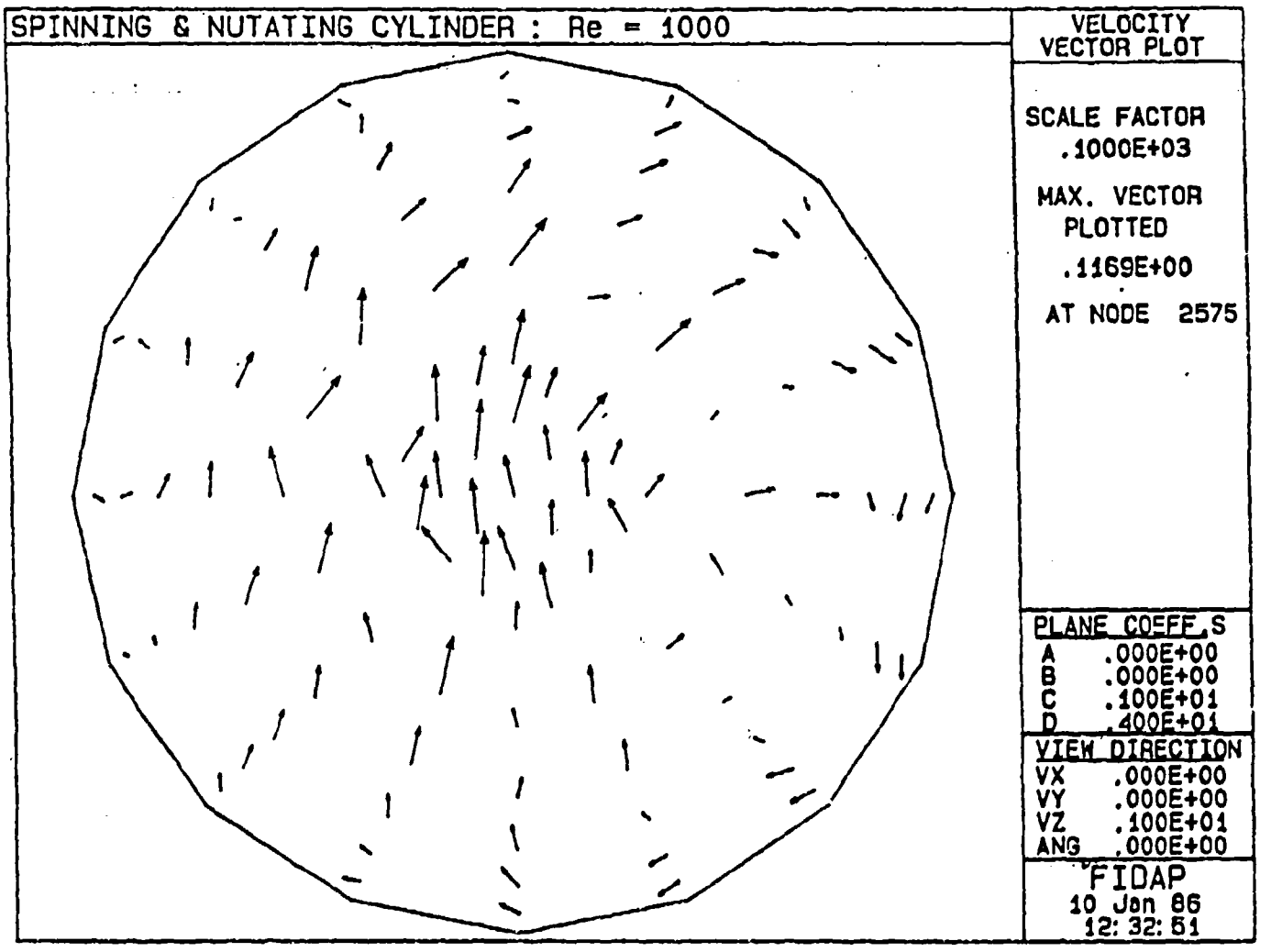
SPINNING & NUTATING CYLINDER : Re = 1000
VELOCITY VECTOR PLOT
SCALE FACTOR
.1000E+03
MAX. VECTOR PLOTTED
.1169E+00
AT NODE 2575
PLANE COEFF.S
A .000E+00
B .000E+00
C .100E+01
D .400E+01
VIEW DIRECTION
VX .000E+00
VY .000E+00
VZ .100E+01
ANG .000E+00
FIDAP
10 Jan 86
12:32:51

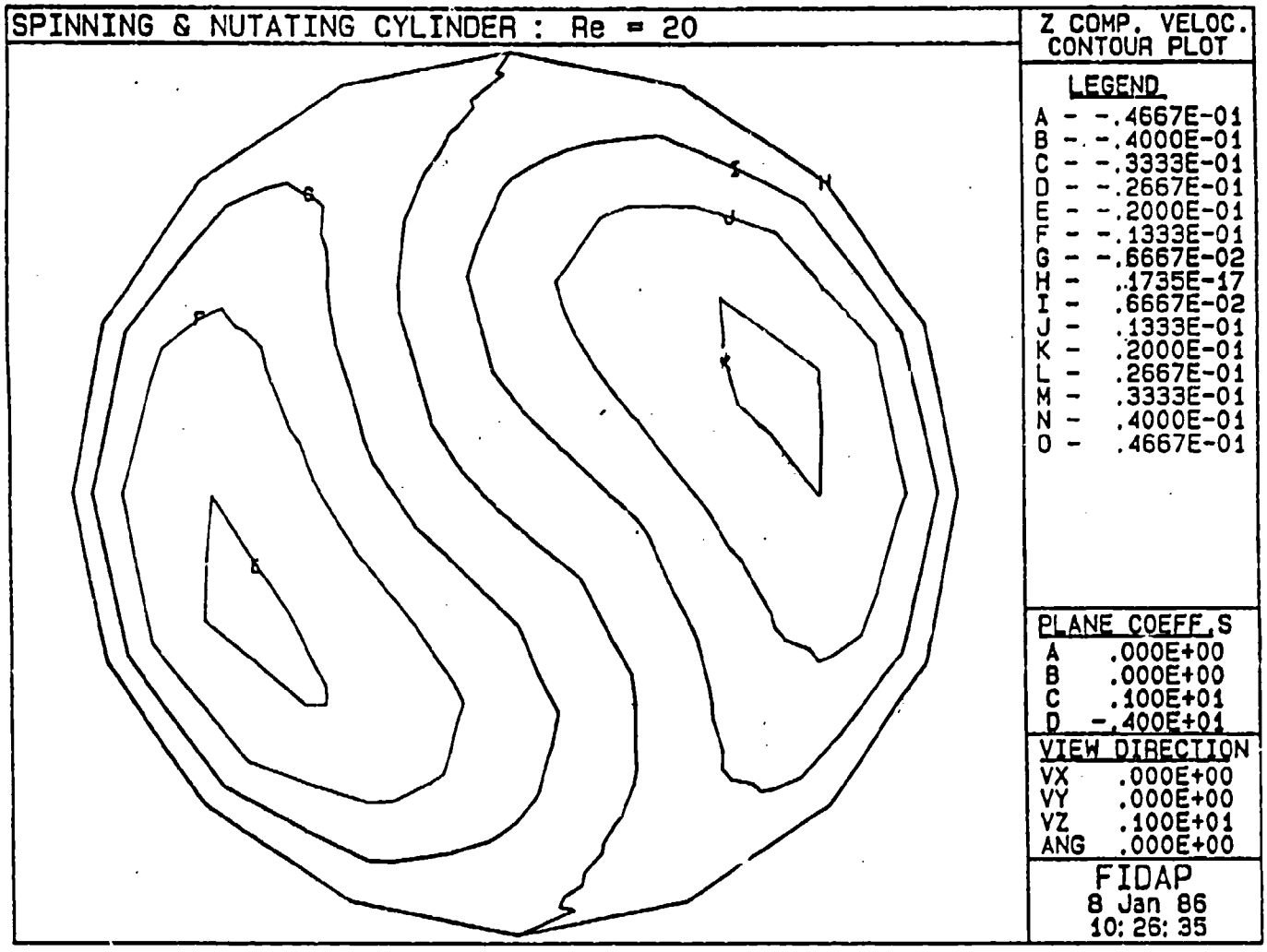
SPINNING & NUTATING CYLINDER : Re = 20
Z COMP. VELOC.
CONTOUR PLOT
LEGEND
A - -.4667E-01
B - -.4000E-01
C - -.3333E-01
D - -.2667E-01
E - -.2000E-01
F - -.1333E-01
G - -.6667E-02
H - .1735E-17
I - .6667E-02
J - .1333E-01
K - .2000E-01
L - .2667E-01
M - .3333E-01
N - .4000E-01
O - .4667E-01
PLANE COEFF.S
A .000E+00
B .000E+00
C .100E+01
D -.400E+01
VIEW DIRECTION
VX .000E+00
VY .000E+00
VZ .100E+01
ANG .000E+00
FIDAP
8 Jan 86
10:26:35

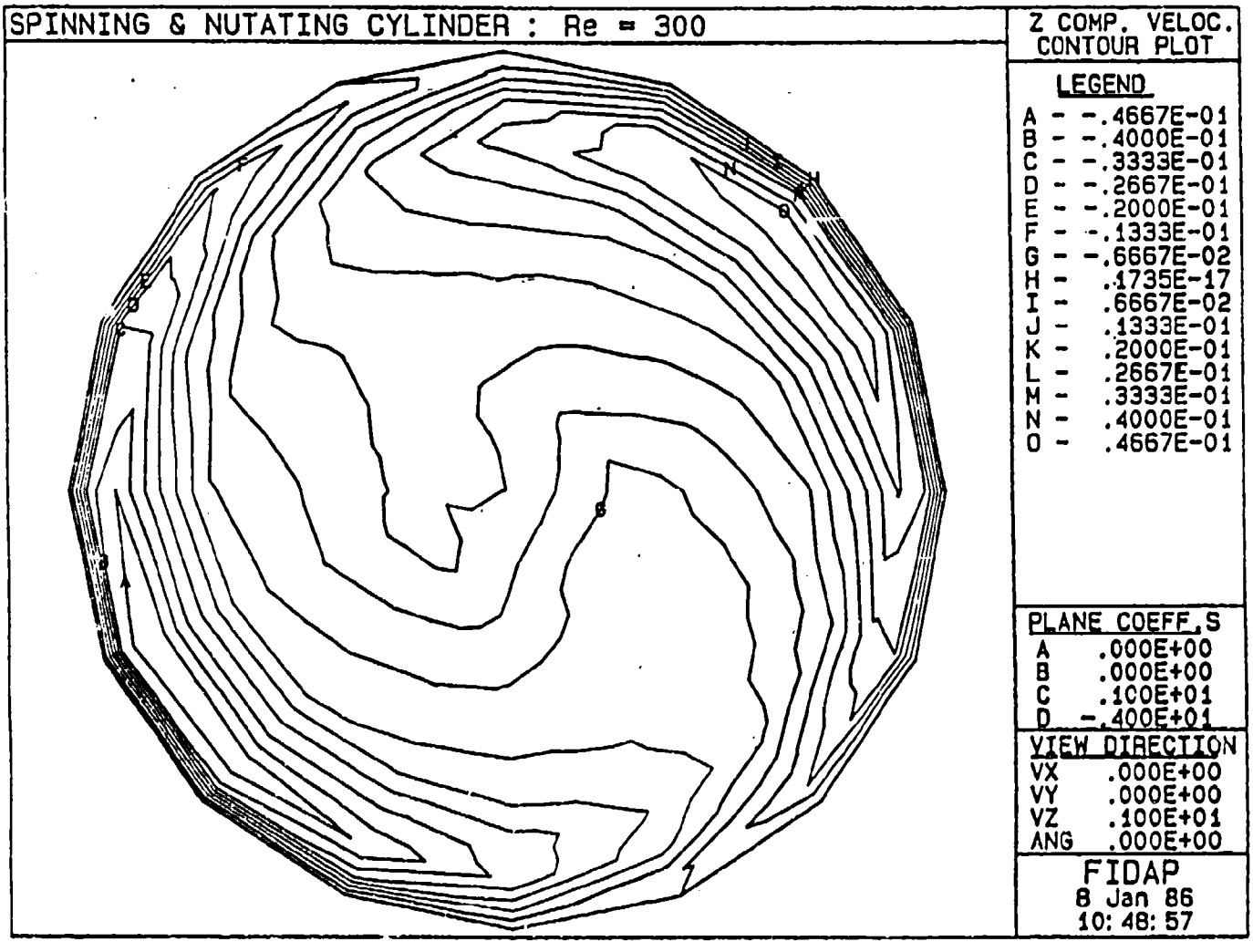
SPINNING & NUTATING CYLINDER : Re = 300
Z COMP. VELOC.
CONTOUR PLOT
LEGEND
A - -.4667E-01
B - -.4000E-01
C - -.3333E-01
D - -.2667E-01
E - -.2000E-01
F - -.1333E-01
G - -.6667E-02
H - .1735E-17
I - .6667E-02
J - .1333E-01
K - .2000E-01
L - .2667E-01
M - .3333E-01
N - .4000E-01
O - .4667E-01
PLANE COEFF,S
A .000E+00
B .000E+00
C .100E+01
D -.400E+01
VIEW DIRECTION
VX .000E+00
VY .000E+00
VZ .100E+01
ANG .000E+00
FIDAP
8 Jan 86
10:48:57

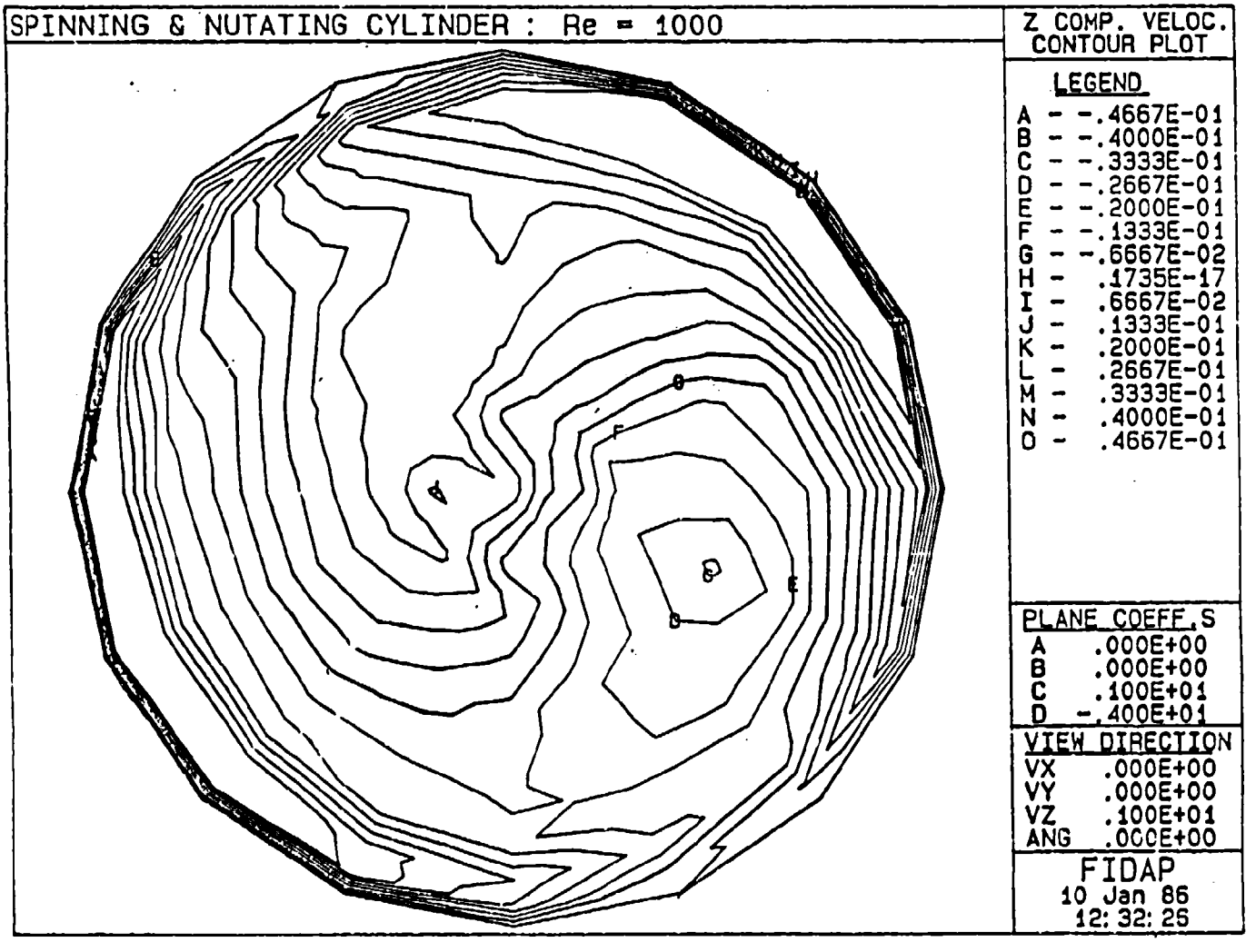
SPINNING & NUTATING CYLINDER : Re = 1000
Z COMP. VELOC.
CONTOUR PLOT
LEGEND
A - -.4667E-01
B - -.4000E-01
C - -.3333E-01
D - -.2667E-01
E - -.2000E-01
F - -.1333E-01
G - -.6667E-02
H - .1735E-17
I - .6667E-02
J - .1333E-01
K - .2000E-01
L - .2667E-01
M - .3333E-01
N - .4000E-01
O - .4667E-01
PLANE COEFF.S
A .000E+00
B .000E+00
C .100E+01
D -.400E+01
VIEW DIRECTION
VX .000E+00
VY .000E+00
VZ .100E+01
ANG .000E+00
FIDAP
10 Jan 86
12:32:25

SPINNING & NUTATING CYLINDER : Re = 20

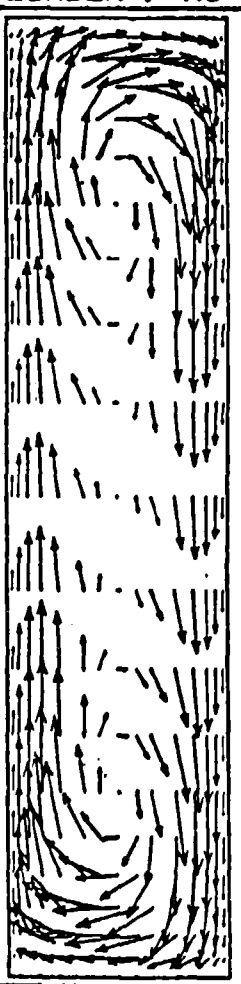

VELOCITY VECTOR PLOT

SCALE FACTOR
.1000E+03

MAX. VECTOR PLOTTED
.5482E-01

AT NODE 626

PLANE COEFF.S	
A	.000E+00
B	.100E+01
C	.000E+00
D	.000E+00

VIEW DIRECTION	
VX	.000E+00
VY	.100E+01
VZ	.000E+00
ANG	.000E+00

FIDAP
8 Jan 86
08:50:30

SPINNING & NUTATING CYLINDER : Re = 300

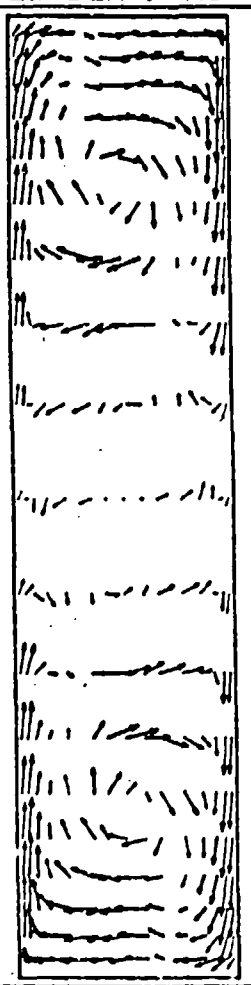

VELOCITY VECTOR PLOT

SCALE FACTOR
.1000E+03

MAX. VECTOR PLOTTED
.1139E+00

AT NODE 545

PLANE COEFF.S	
A	.000E+00
B	.100E+01
C	.000E+00
D	.000E+00

VIEW DIRECTION	
VX	.000E+00
VY	.100E+01
VZ	.000E+00
ANG	.000E+00

FIDAP
C Jan 86
08:29:01

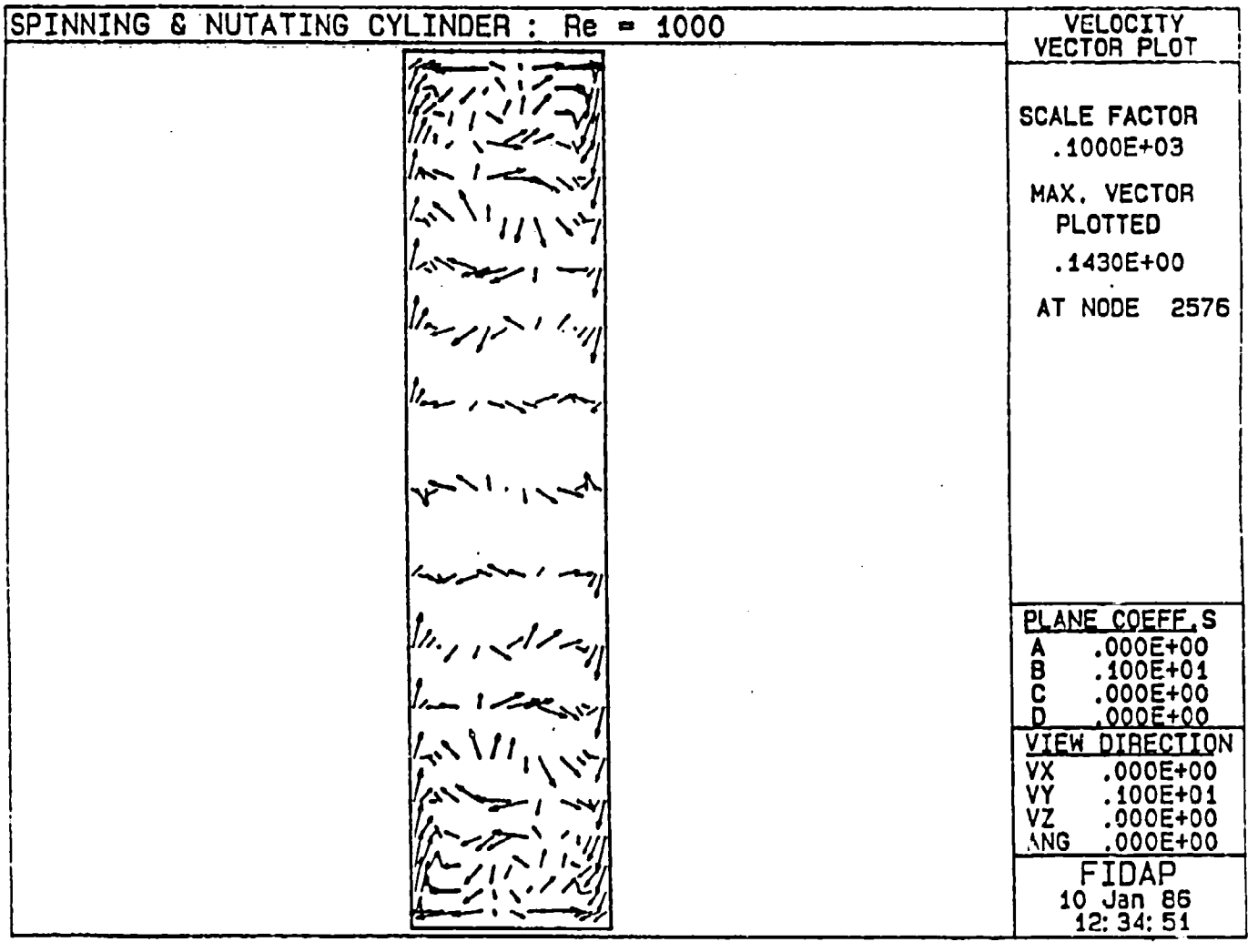
SPINNING & NUTATING CYLINDER : Re = 1000
VELOCITY VECTOR PLOT
SCALE FACTOR
.1000E+03
MAX. VECTOR PLOTTED
.1430E+00
AT NODE 2576
PLANE COEFF.S
A .000E+00
B .100E+01
C .000E+00
D .000E+00
VIEW DIRECTION
VX .000E+00
VY .100E+01
VZ .000E+00
ANG .000E+00
FIDAP
10 Jan 86
12:34:51

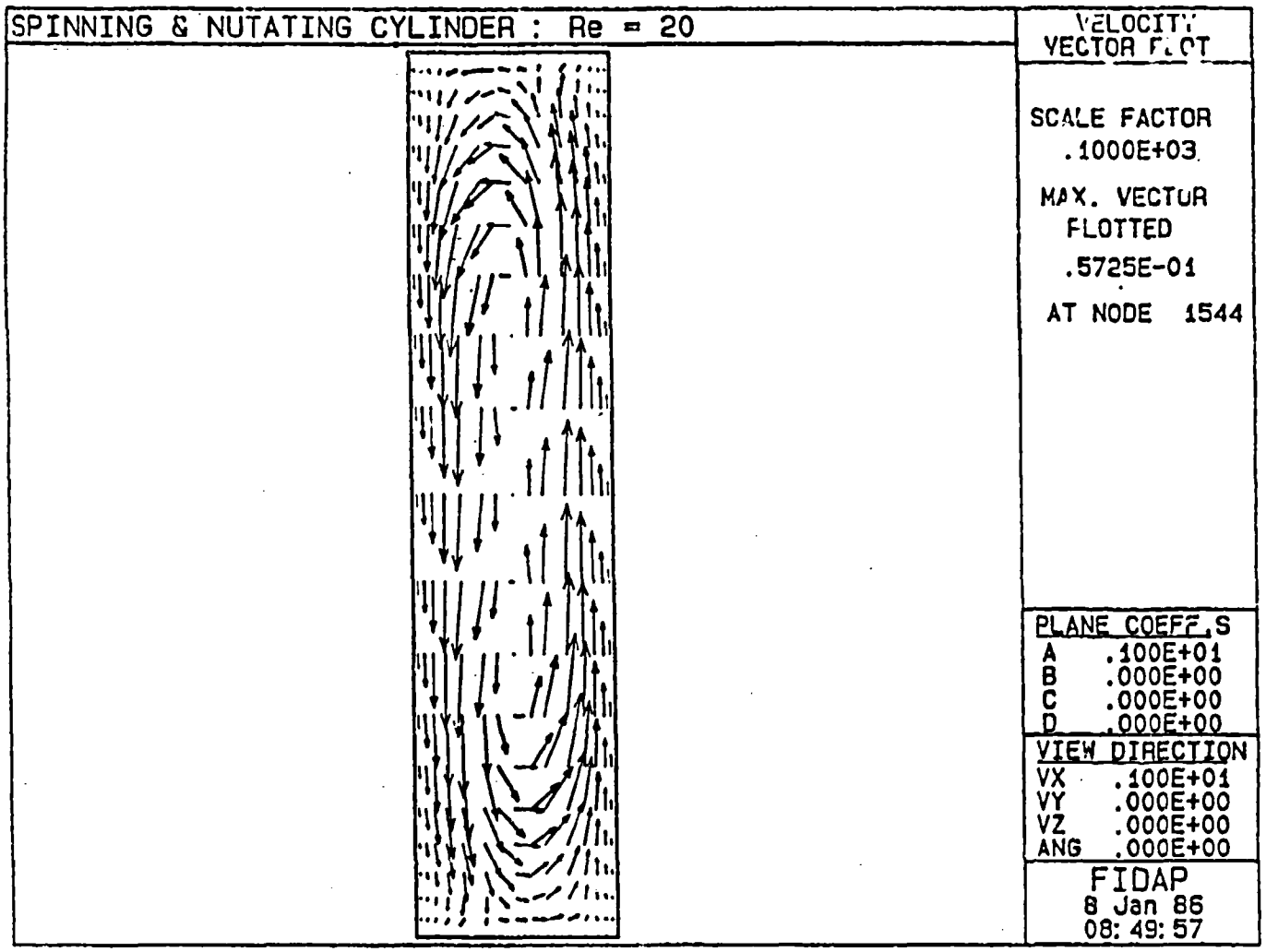
SPINNING & NUTATING CYLINDER : Re = 20
VELOCITY VECTOR PLOT
SCALE FACTOR
.1000E+03
MAX. VECTOR FLOTTED
.5725E-01
AT NODE 1544
PLANE COEFF.S
A .100E+01
B .000E+00
C .000E+00
D .000E+00
VIEW DIRECTION
VX .100E+01
VY .000E+00
VZ .000E+00
ANG .000E+00
FIDAP
8 Jan 86
08:49:57

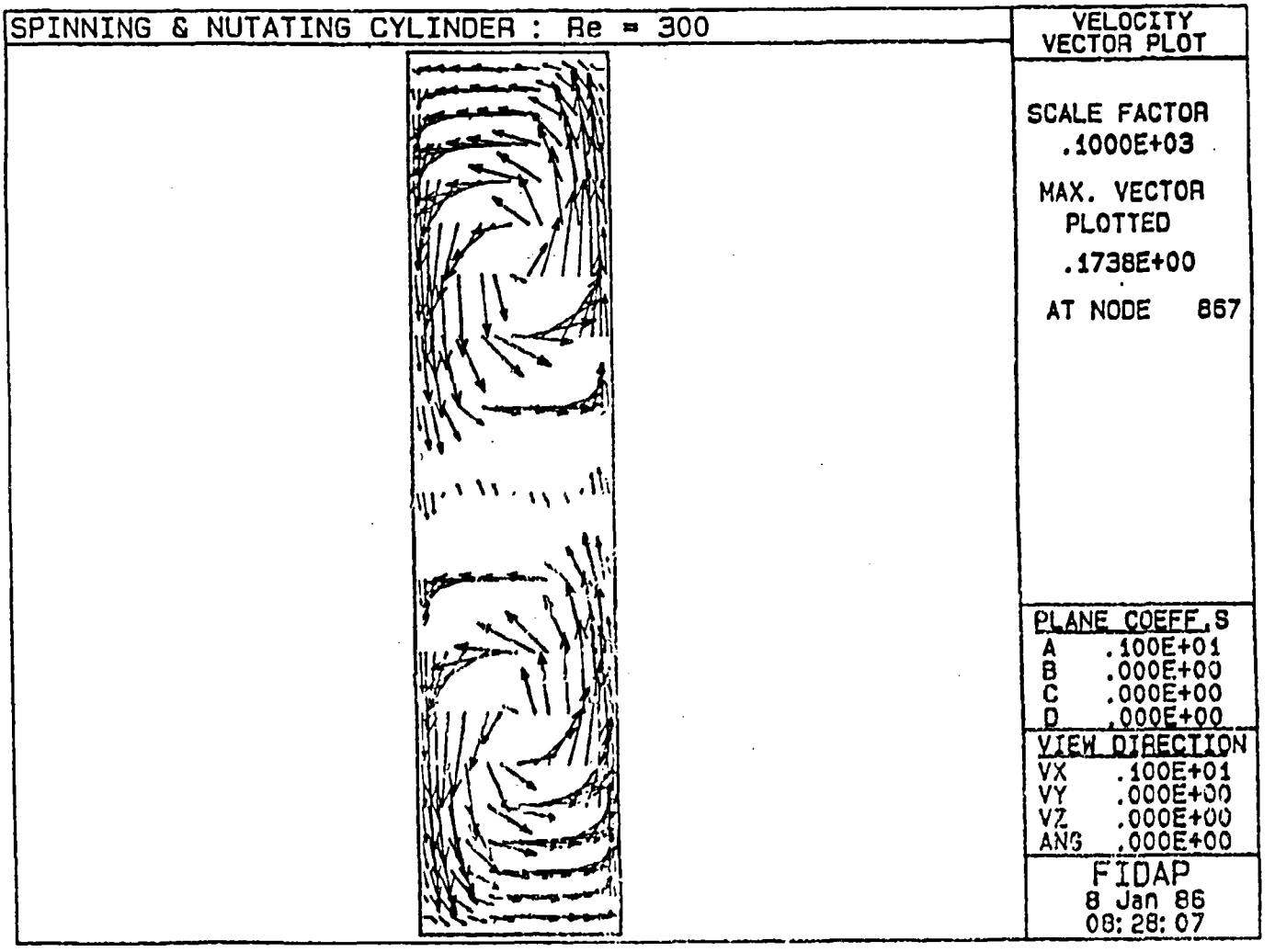
SPINNING & NUTATING CYLINDER : Re = 300
VELOCITY VECTOR PLOT
SCALE FACTOR
.1000E+03
MAX. VECTOR PLOTTED
.1738E+00
AT NODE 867
PLANE COEFF.S
A .100E+01
B .000E+00
C .000E+00
D .000E+00
VIEW DIRECTION
VX .100E+01
VY .000E+00
VZ .000E+00
ANG .000E+00
FIDAP
8 Jan 86
08:28:07

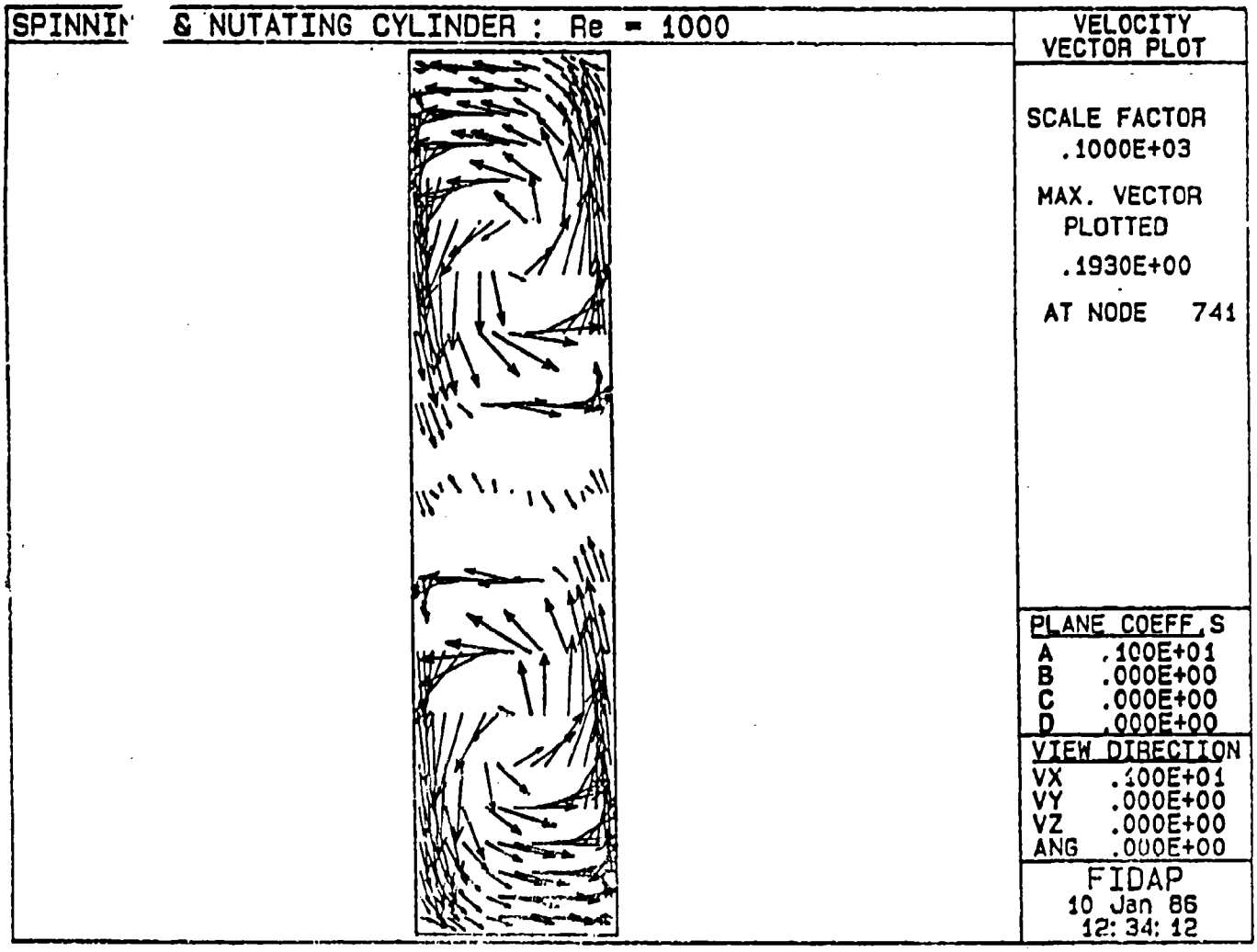
SPINNI
& NUTATING CYLINDER : Re = 1000
VELOCITY VECTOR PLOT
SCALE FACTOR
.1000E+03
MAX. VECTOR PLOTTED
.1930E+00
AT NODE 741
PLANE COEFF.S
A .100E+01
B .000E+00
C .000E+00
D .000E+00
VIEW DIRECTION
VX .100E+01
VY .000E+00
VZ .000E+00
ANG .000E+00
FIDAP
10 Jan 86
12:34:12

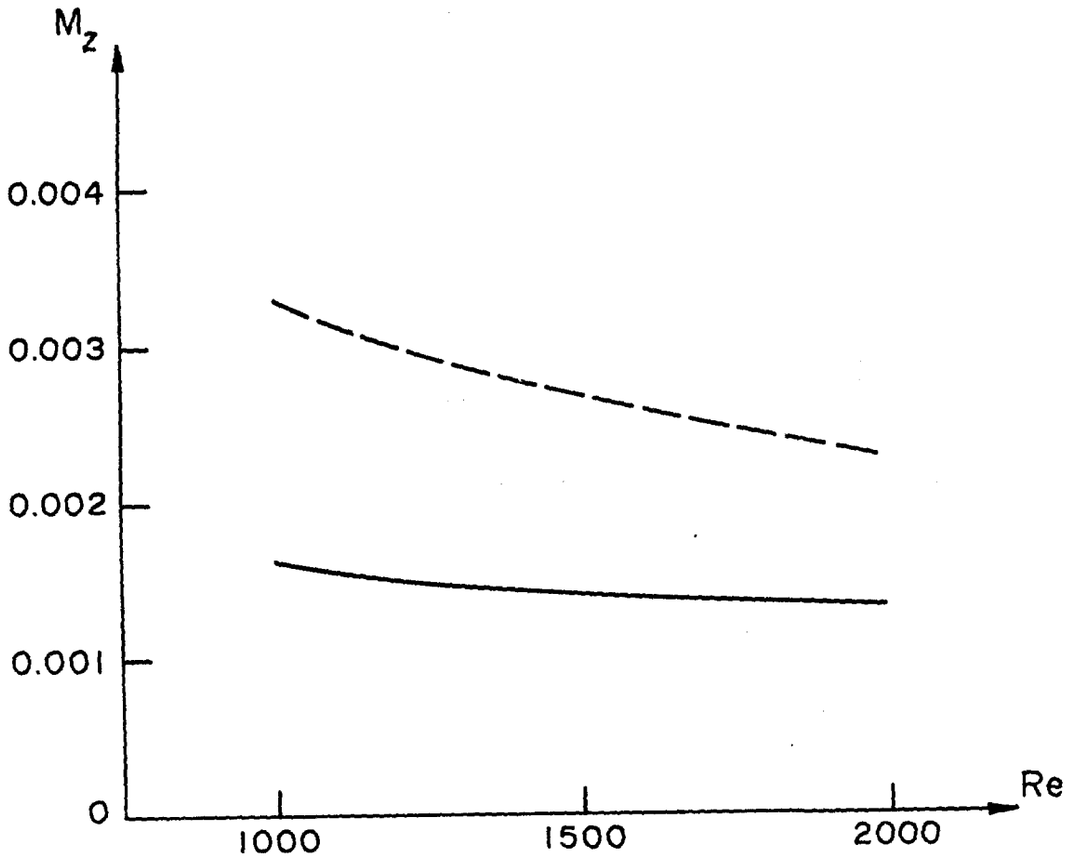

Figure 19: Variation of despin moment M_z with Reynolds number for non-Newtonian Liquid 1 (solid curve) and for an equivalent Newtonian liquid (broken curve) with Ω = 400 rpm, ω = 4000 rpm, θ = 20°

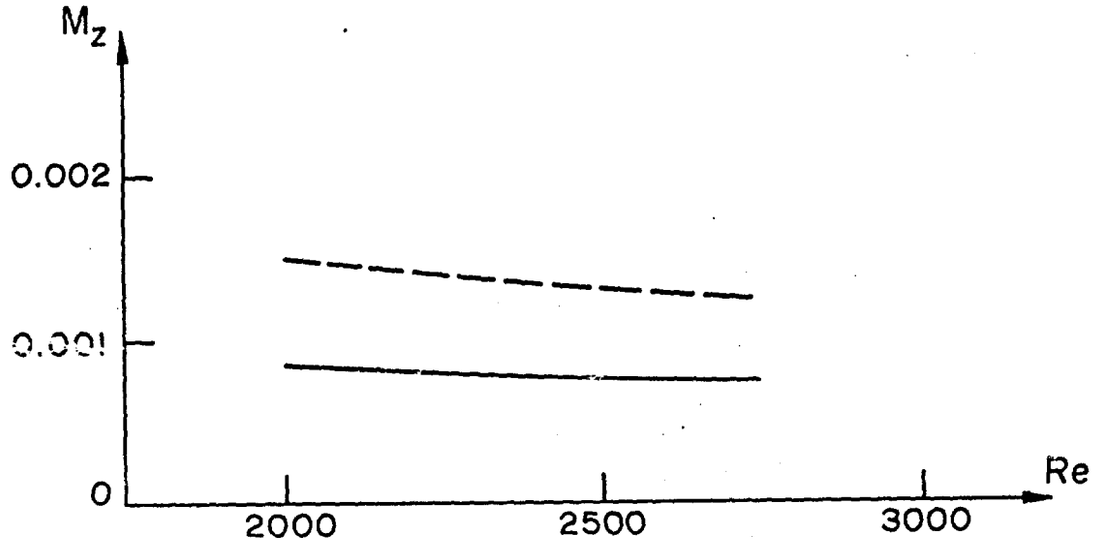

Figure 10. Variation of desp. n moment M_z with Reynolds number for non-Newtonian Liquid 1 (solid curve) and for an equivalent Newtonian liquid (broken curve) with Ω = 400 rpm, ω = 4800 rpm, θ = 20°

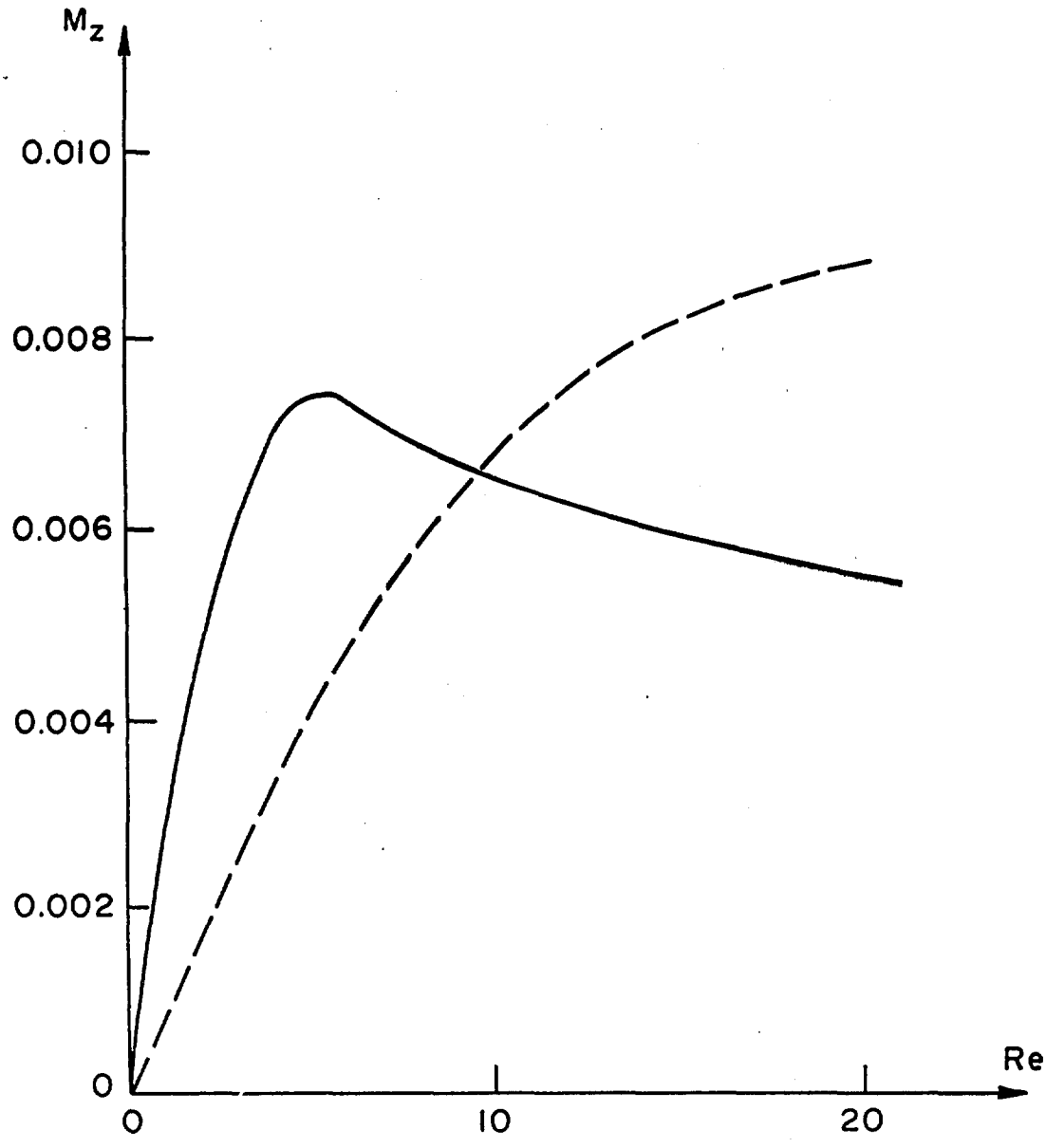

Figure 21: Variation of despin moment M_z with Reynolds number for non-Newtonian Liquid 2 (solid curve) and for an equivalent Newtonian liquid (broken curve) with Ω = 400 rpm, ω = 4000 rpm, θ = 20°

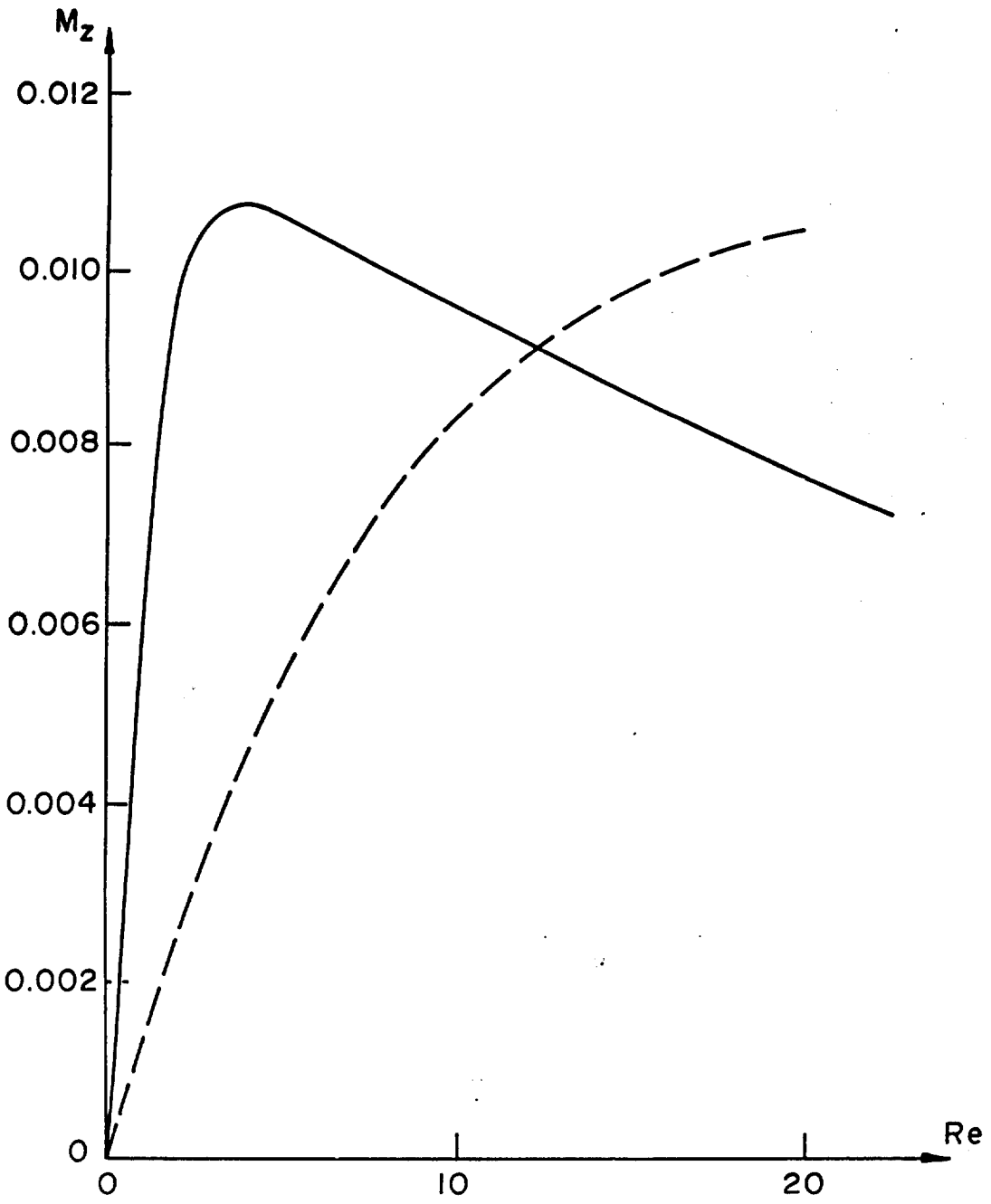

Figure 22: Variation of despin moment M_z with Reynolds number for non-Newtonian Liquid 2 (solid curve) and for an equivalent Newtonian liquid (broken curve) with Ω = 400 rpm, ω = 4800 rpm, θ = 20°

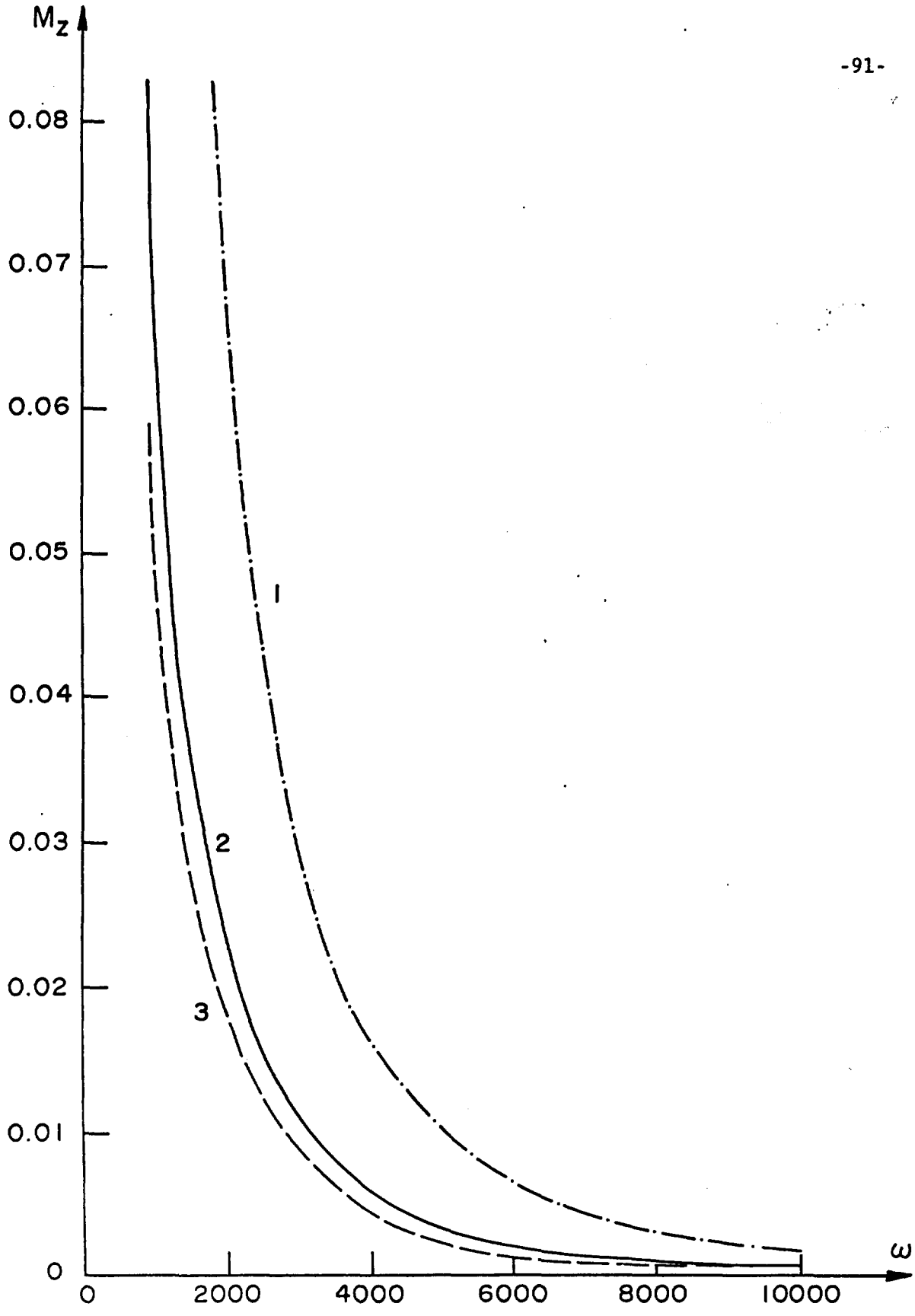

Figure 23: Variation of M_z with spin rate ω for Liquid 2

1. Ω = 500 rpm, θ = 20°
2. Ω = 300 rpm, θ = 20°
3. Ω = 500 rpm, θ = 10°